

Circumstellar Disk Lifetimes In Numerous Galactic Young Stellar Clusters

A. J. W. Richert,¹ K. V. Getman,^{1*} E. D. Feigelson,¹ M. A. Kuhn,^{2,3}
P. S. Broos,¹ M. S. Povich,⁴ M. R. Bate,⁵ G. P. Garmire⁶

¹*Department of Astronomy & Astrophysics, 525 Davey Laboratory, Pennsylvania State University, University Park PA 16802*

²*Instituto de Física y Astronomía, Universidad de Valparaíso, Gran Bretaña 1111, Playa Ancha, Valparaíso, Chile*

³*Millennium Institute of Astrophysics, Av. Vicuña Mackenna 4860, 782-0436 Macul, Santiago, Chile*

⁴*Department of Physics and Astronomy, California State Polytechnic University, 3801 West Temple Ave, Pomona, CA 91768*

⁵*Department of Physics and Astronomy, University of Exeter, Stocker Road, Exeter, Devon EX4 4QL, UK*

⁶*Huntingdon Institute for X-ray Astronomy, LLC, 10677 Franks Road, Huntingdon, PA 16652, USA*

Accepted for publication in MNRAS, 2018 April 11

ABSTRACT

Photometric detections of dust circumstellar disks around pre-main sequence (PMS) stars, coupled with estimates of stellar ages, provide constraints on the time available for planet formation. Most previous studies on disk longevity, starting with Haisch, Lada & Lada (2001), use star samples from PMS clusters but do not consider datasets with homogeneous photometric sensitivities and/or ages placed on a uniform timescale. Here we conduct the largest study to date of the longevity of inner dust disks using X-ray and 1–8 μm infrared photometry from the MYStIX and SFINC projects for 69 young clusters in 32 nearby star-forming regions with ages $t \leq 5$ Myr. Cluster ages are derived by combining the empirical Age_{JX} method with PMS evolutionary models, which treat dynamo-generated magnetic fields in different ways. Leveraging X-ray data to identify disk-free objects, we impose similar stellar mass sensitivity limits for disk-bearing and disk-free YSOs while extending the analysis to stellar masses as low as $M \sim 0.1 M_{\odot}$. We find that the disk longevity estimates are strongly affected by the choice of PMS evolutionary model. Assuming a disk fraction of 100% at zero age, the inferred disk half-life changes significantly, from $t_{1/2} \sim 1.3 - 2$ Myr to $t_{1/2} \sim 3.5$ Myr when switching from non-magnetic to magnetic PMS models. In addition, we find no statistically significant evidence that disk fraction varies with stellar mass within the first few Myr of life for stars with masses $< 2 M_{\odot}$, but our samples may not be complete for more massive stars. The effects of initial disk fraction and star-forming environment are also explored.

Key words: infrared: stars – stars: early-type – open clusters and associations: general – stars: formation – stars: pre-main sequence – X-rays: stars

1 INTRODUCTION

The time required to assemble planets in young circumstellar disks remains a key variable in planet formation theory. Given that planets form out of gas and dust in young circumstellar disks following protostellar collapse, observed lifetimes of the gas and dust phases translate into constraints on the time available to form Jovian and terrestrial planets, respectively (Youdin & Goodman 2005; Lyra et al. 2008; Boss 2010). Measuring disk lifetimes also plays a role in constraining models of disk evolution more generally, as disk material is depleted by accretion onto the star, internal and external

photoevaporation, disk winds, and planetesimal and planet formation (Lynden-Bell & Pringle 1974; Pringle 1981; Bell et al. 1997; Armitage 2011; Bai 2011; Königl & Salmeron 2011). Since disk evolution may be dominated by turbulent viscosity, observationally-derived disk lifetimes are often used to estimate characteristic viscous α values (Shakura & Sunyaev 1973).

Alpha-disk theory allows a disk to be long-lived or short-lived depending on the unknown viscosity (Armitage 2011), therefore in the absence of robust theoretical constraints on effective α values, the actual distribution of longevities for an ensemble of disks must be evaluated observationally. In principle, initial disk masses and disk depletion rates for individual systems could be used to estimate disk lifetimes,

* E-mail: kug1@psu.edu (KVG)

however initial disk masses cannot be retrospectively determined for individual systems, and there is no reason to assume that disk dissipation rates are constant over the long lifetime of a disk. In fact, there is strong evidence that accretion rates are fast during the protostellar phase and slow during later PMS phases, and may be variable on shorter timescales as well (Bouvier et al. 1993; Alencar et al. 2010; Audard et al. 2014; Cody et al. 2014). Therefore, the study of disk longevity typically relies on disk population statistics rather than observations of individual systems.

The earliest empirical study of disk longevity was carried out by Strom et al. (1989), who found that the fraction of stars with hot inner accretion disks, detected by K -band excess and $H\alpha$ emission (associated with classical T-Tauri stars), diminishes significantly for stars older than 3 Myr in the Taurus–Auriga star-forming region.

In the seminal study of Haisch et al. (2001b), the authors plot the fraction of stars showing L -band excess, indicating a hot inner dust disk, as a function of age for several young-to-intermediate age clusters (2.5–30 Myr). They identify a clear trend wherein disks are depleted over the course of several million years. This basic methodology of comparing cluster disk fraction with average stellar age has been adopted by a number of groups for more clusters spanning a wider age range (Hernández et al. 2008; Mamajek 2009; Fedele et al. 2010; Bell et al. 2013; Ribas et al. 2014). In some cases, multiple disk indicators are used; Mamajek (2009), for instance, uses $H\alpha$ emission, L -band excess, $3.6\ \mu\text{m}$ excess, and infrared spectral energy distribution (SED) shape as indicators of the presence of a hot inner disk. There is some evidence that disk longevity depends on host star spectral type (e.g., Haisch et al. 2001a; Hernández et al. 2005; Carpenter et al. 2006; Kennedy & Kenyon 2009; Hernández et al. 2010; Luhman & Mamajek 2012; Ribas et al. 2015), with higher-mass stars appearing to shed their disks more quickly.

Fedele et al. (2010) consider the possibility that the dust and gas of a disk do not perfectly coevolve. They compare the fraction of young stellar objects (YSOs) showing spectroscopic evidence of accretion onto the star ($H\alpha$ emission) with the fraction showing infrared excess in *Spitzer*/IRAC bands (3.6 – $8.0\ \mu\text{m}$, revealing small grains in the inner several AU of a disk). Exponential half-lives calculated based on spectroscopic signs of accretion are slightly shorter than those calculated based on infrared excess. This indicates that circumstellar gas and dust mostly coevolve, but that disks may retain a longer-lived dusty component after the gas has been depleted.

One potentially significant limitation of some previous works is the differing sensitivity limits between disk-bearing and disk-free YSOs. Disk-bearing YSOs are usually detected through infrared excess, therefore point source catalogs compiled using infrared photometry are biased toward finding disk-bearing YSOs. An overestimation of disk fraction will translate into an overestimation of disk lifetimes. This effect may be particularly important among lower-mass (i.e., intrinsically fainter) stars, potentially leading to an apparent mass dependency that is not physical.

Another major impediment to obtaining accurate disk dissipation timescales is the absence of a reliable stellar chronometer. Ages of individual PMS stars as well as age spreads of PMS members in individual clusters and star-

forming regions are not accurate due to an interplay of multiple factors, such as photometric variability from accretion and magnetic activity, different accretional histories, binarity, extinction uncertainty, veiling from accretion, scattering and absorption by disks, stellar interiors model uncertainties including inconsistent age predictions for intermediate-mass and lower-mass stars, distance uncertainty, and others (e.g. Preibisch 2012; Getman et al. 2014; Jeffries 2017).

Recent empirical evidence points to persistent errors in standard theoretical PMS evolutionary models, both old generation, such as Baraffe et al. (1998); Siess et al. (2000), and new generation, such as Baraffe et al. (2015); Dotter (2016); Choi et al. (2016). This emerges independently from: findings of inconsistent ages between intermediate-mass and low-mass stars (Pecaut & Mamajek 2016; Fang et al. 2017) derived from the Hertzsprung-Russell diagram (HRD) or photometric color-magnitude diagram (CMD); failure of theoretical models to reproduce the observed parameters of stars in eclipsing binaries (Kraus et al. 2015); and disagreement between Li-based and HRD/CMD-based ages (Jeffries et al. 2017). Specifically, the HRD locations of observed eclipsing binaries suggest that theoretical models underpredict (by 5 – 20%) the stellar radii and overpredict T_{eff} (by 5 – 10%) of low-mass ($M < 1\ M_{\odot}$) PMS and MS stars, a phenomenon referred to as “radius inflation”. Empirical correlations of inflation with rotation and magnetic activity (Somers & Stassun 2017) suggest that magnetic fields drive radius inflation. Recent attempts to account for magnetic effects include two types of models: global magnetic fields threaded into the stellar interior (Feiden 2016) and starspot flux blocking (Somers & Pinsonneault 2015). Both models lead to changes in the stellar structure that reproduce true radius sizes.

Some of the previous works on cluster disk fraction including Haisch et al. (2001b); Hernández et al. (2008); Mamajek (2009); Fedele et al. (2010); Ribas et al. (2014) employ literature compilations of heterogeneous sets of cluster members and/or heterogeneous estimates of cluster ages. Examples of obvious sources of heterogeneity, which lead to uncertainty and scatter in age estimates, include differing data wavelength ranges, types of data (e.g., photometry versus spectroscopy), age methods (e.g., HRD, CMD, disk fraction, kinematic, etc.), stellar mass ranges, ways of transformation between theory and observation, subcluster membership in star-forming regions and others (e.g., Soderblom et al. 2014). Application of differing PMS evolutionary models to the same set of data would generally lead to systematic shifts in age estimates. None of the aforementioned studies considered the impact of differing PMS models on their disk longevity estimates.

To investigate some of the aforementioned issues in detail, we employ the data from the Massive Young Star-Forming Complex Study in Infrared and X-ray (MYStIX, Feigelson et al. 2013) and Star Formation in Nearby Clouds (SFINC, Getman et al. 2017) projects. Both datasets incorporate *Chandra* X-ray data to help identify disk-free YSOs in 42 total young star-forming regions (SFRs). In the current work, we use YSO classifications (disk-bearing versus disk-free) of X-ray and infrared point sources along with homogeneous sets of cluster ages (Getman et al. 2014) for 69 clusters spread across 32 of the total 42 MYStIX and

SFiNCs target regions (Kuhn et al. 2014; Getman et al. 2018) to study effects of differing PMS evolutionary models, mass, star-forming environments, and initial disk fractions on disk longevity. Ten MYStIX/SFiNCs regions without cluster membership assignments and/or sufficient numbers of stars with available age estimates and disk classes were excluded from our disk fraction analyses (§2.1).

YSO candidate selection and cluster membership determination are described in Section 2.1. The classification of disk-bearing and disk-free YSOs is summarized in Section 2.2. Age estimation for MYStIX and SFiNCs clusters using multiple PMS evolutionary models is given in Section 2.3. Our strategy for mitigating the problem of differential mass sensitivities for disk-bearing and disk-free YSOs is discussed in Section 2.4. The main results for disk longevity are discussed in Section 3, including the impacts of different factors (classification of YSOs on disk-bearing and disk-free, assumption of initial disk fraction, choice of PMS model, effects of stellar star-forming environments and mass) on our disk longevity estimates. Further discussion, comparison with previous literature, and suggestions for future work are presented in Section 4.

2 METHODS

2.1 Cluster membership

The MYStIX probable cluster member catalog contains cross-matched X-ray (*Chandra*/ACIS), near-infrared (2MASS or UKIDSS), and mid-infrared (*Spitzer*/IRAC; 3.6–8.0 μm) point sources. Infrared excess (IRE) selection captures PMS stars with hot inner disks while X-ray selection captures PMS stars with strong magnetic flaring activity. IRE stars are found by comparing the 1–8 μm spectral energy distributions to circumstellar disk models (Povich et al. 2013) while X-ray stars are found with a naive Bayes classifier that takes a variety of properties into account (Broos et al. 2013). Generally in MYStIX, the *Chandra* samples are larger than the IRE samples, but there is often considerable overlap in members identified by the two methods. Detailed discussion of catalog assembly and membership selection is provided by Feigelson et al. (2013) and other MYStIX papers (Kuhn et al. 2013a,b; Naylor et al. 2013; Povich et al. 2013; Townsley et al. 2014). The full list of ~ 32000 MYStIX probable YSO members is given by Broos et al. (2013); and Kuhn et al. (2014) identify 142 clusters across 17 MYStIX regions by fitting isothermal ellipsoids to the star locations.

The same MYStIX-based X-ray and IR data analysis methods are used for the reanalysis of the archived *Chandra* and *Spitzer* data for the nearby 22 SFiNCs SFRs (Getman et al. 2017). Due to the smaller cluster distances and higher Galactic latitudes of the SFiNCs SFRs compared to MYStIX ones, the IR counterpart and YSO membership identifications are achieved using simpler methods than in MYStIX, such as traditional proximity and decision tree membership classification methods (Getman et al. 2017). The full list of nearly 8,500 SFiNCs probable YSO members is given by Getman et al. (2017). Getman et al. (2018) identify 52 clusters and 19 unclustered stellar structures across the 22 SFiNCs SFRs using the methods of Kuhn et al. (2014). For our disk longevity analysis, the 19 unclustered stellar structures are each treated as a single cluster. Throughout the

remainder of this paper, the term “cluster” will also apply to these 19 unclustered components.

Sensitivity and completeness levels of the MYStIX and SFiNCs YSO catalogs vary among the regions due to differing distances, observation exposures, and absorptions across the fields, as well as due to differing levels of diffuse IR nebular background. For instance, the very deep X-ray exposure of the nearby ONC cluster reaches the completeness limits of $\sim 0.1\text{--}0.2 M_{\odot}$, while the deep X-ray exposure of the most distant MYStIX region NGC 1893 allows a nearly complete detection of PMS stars only above $\sim 1\text{--}2 M_{\odot}$ (see Figure 1 in Kuhn et al. 2015a). For more distant ($d > 1$ kpc) MYStIX regions, the 2MASS limiting sensitivity of $K_s \sim 14.3$ mag becomes inadequate for identifying YSO counterparts to *Chandra* sources; thus for most of these regions, the 2MASS catalog is complemented by the deeper UKIRT catalog, when available (Feigelson et al. 2013). The *Chandra* X-ray-selected and *Spitzer* mid-infrared-selected MYStIX/SFiNCs YSO samples generally have different sensitivities within individual regions; for instance, an X-ray selected YSO portion is deeper for Be 59 (see Figure 12 in Getman et al. 2017), but a mid-infrared-selected portion is deeper for W 40 (see Figure 8 in Kuhn et al. 2015b).

Due to the omission of *Spitzer*-MIPS and far-infrared data, MYStIX and SFiNCs lack the ability to identify some fraction of protostellar objects and transition disk objects (systems with inner disk holes or optically thin inner disks), especially those that were not detected in X-rays. Since the ages of the MYStIX and SFiNCs clusters are estimated based on PMS samples (§2.3), we are instead interested in characterization of disk fractions for YSO samples, from which the remaining protostars are removed (§2.2).

The membership algorithms applied to the MYStIX and SFiNCs X-ray, NIR, and MIR catalogs produce small fractions of false positives. For instance, Table 8 in Broos et al. (2013) shows an excellent (within a few to several percent) agreement between the numbers of the simulated and identified and removed extragalactic and Galactic field contaminants. Getman et al. (2017) estimate that less than a few percent of contaminants, mainly field stars, could be present within the SFiNCs sample of young stellar objects. Getman et al. further compare SFiNCs with previously published YSO catalogs. As an example of the low contamination in SFiNCs membership, here we consider IC 348, one of the richest nearby star-forming regions. Table 9 and Figures 12, 17, and 18 in Getman et al. show that the SFiNCs YSO identification is in good agreement with the recent optical/infrared spectroscopic/photometric YSO catalog of (Luhman et al. 2016, hereafter Lu16). Out of the 478 Lu16 YSOs, 77% are identified by SFiNCs. Half of the remaining 23% (generally IR brighter) lie outside the SFiNCs X-ray fields, and the other half (IR weaker) are very low-mass stellar and brown dwarf candidates ($M \lesssim 0.1 M_{\odot}$) undetectable in the SFiNCs X-ray exposures. On the other hand, additional to Lu16, SFiNCs identifies 29 new YSOs; of those half are disk-free and half are disk-bearing; over two-thirds are X-ray detected. The fact that the vast majority of these are not distributed randomly across the SFiNCs X-ray field but are rather spatially concentrated in the southern part of the field, right outside the primary membership area of Lu16 ($r = 14'$; their Figure 1), and have IR/X-ray colors con-

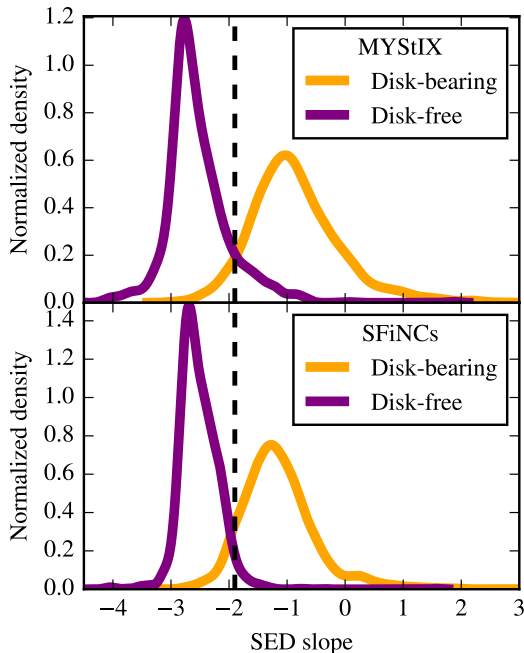


Figure 1. Kernel density estimation of SED slopes α_{IRAC} for MYStIX (upper panel) and SFiNCs (lower panel) YSOs.

sistent with those of the other YSOs, gives confidence that these are real YSOs and not source contaminants.

Only a portion of the full MYStIX and SFiNCs samples can be used for our effort to understand disk evolution. Specifically, we require clusters with available Age_{JX} estimates (Section 2.3) and at least 10 disk-bearing and 10 disk-free YSOs within each cluster *prior* to the imposition of mass cuts described in Section 2.4. The resulting subsample consists of 7,100 MYStIX YSOs in 34 clusters, and 5,834 SFiNCs YSOs in 35 clusters. These numbers of YSOs are further reduced after the imposition of mass cuts (Section 2.4); and the numbers vary among the four different membership permutations considered in the current study (Section 2.2). The final YSO numbers are listed in Tables 1 and 2.

2.2 YSO classification

There is no consensus on criteria for discriminating between disk-bearing and disk-free stars. We apply and compare two schemes for doing so. In the first, we use the classifications found in the MYStIX and SFiNCs catalogs derived in the following ways. For MYStIX, Povich et al. (2013) classify YSOs by fitting JHK_s and *Spitzer*/IRAC photometry with the model spectral energy distributions of Robitaille et al. (2006, disks) and Castelli & Kurucz (2004, stellar photospheres), and removing numerous contaminating sources (extragalactic objects, asymptotic giant branch stars, nebular knots, and unrelated YSOs) through additional infrared color cuts and spatial clustering analyses. X-ray detections, an indicator of youth, are required for disk-free YSOs in order to exclude field stars. SFiNCs regions are out of the Galactic plane and therefore suffer from less contamination than MYStIX regions. Getman et al. (2017)

therefore classify SFiNCs YSOs using simpler procedures, namely, the *Spitzer*/IRAC color-color diagram scheme of Gutermuth et al. (2009) combined with the SED-based analysis of Getman et al. (2012). We refer to this first set of YSO classifications collectively as “catalog class.”

Our second YSO classification scheme is based on apparent (non-dereddened) *Spitzer*/IRAC SED slopes, $\alpha_{IRAC} = d \log(\lambda F_\lambda) / d \log(\lambda)$, measured in the IRAC wavelength range from 3.6 to 8.0 μm . Available magnitudes in the 3.6, 4.5, 5.8, and 8.0 μm bands were used for the calculation of 100%, 100%, 64%, and 49% of the SED slopes, respectively. We use a critical value of $\alpha_{IRAC} = -1.9$ to distinguish between disk-bearing and disk-free YSOs. In Fig. 1, we plot kernel density distributions of α_{IRAC} for MYStIX and SFiNCs, separately for disk-bearing and disk-free objects as determined by catalog class (discussed in the previous paragraph). In both figures, the crossover point between disk-bearing and disk-free is close to -1.9 . For MYStIX, 91% of disk-bearing YSOs have $\alpha_{IRAC} > -1.9$, while 86% of disk-free YSOs have $\alpha_{IRAC} < -1.9$. For SFiNCs, 91% of disk-bearing YSOs have $\alpha_{IRAC} > -1.9$, while 96% of SFiNCs disk-free YSOs have $\alpha_{IRAC} < -1.9$. The separation between disk-bearing and disk-free objects therefore appears to be consistent between MYStIX and SFiNCs. The two YSO classification schemes disagree for $< 14\%$ ($< 9\%$) of the MYStIX (SFiNCs) stars.

For both YSO classification schemes, we repeat our analysis (presented in § 3) while excluding probable protostars. We define probable protostars as being those objects with (non-dereddened) $\alpha_{IRAC} > 0$.

We utilize both of the aforementioned schemes not only to compare these approaches—model SED-fitting, color-color diagrams, and infrared slope-based classifications are all widely used in the literature—but also due to the fact that model SED fitting and color-color based schemes yield many ambiguous classifications, including due to transition disks. The latter typically show weak or no IR excesses in the IRAC bands, adding to the uncertainties in disk classification and resulting disk fraction.

2.3 Cluster ages

MYStIX and SFiNCs cluster ages are determined using the Age_{JX} method described by Getman et al. (2014). Age_{JX} is applicable only to low-mass PMS stars ($M < 1.2 M_\odot$ assuming the Siess et al. (2000) age scale) with reliable measurements of the intrinsic X-ray luminosity and near-infrared JHK_s photometry. X-ray luminosities (L_X) specify stellar mass according to the empirical PMS correlation seen in the Taurus region (Telleschi et al. 2007). J -band luminosities and mass estimates track with PMS evolutionary models, providing stellar ages. This yields homogeneous median age estimates for all 69 clusters used in the current analysis. To investigate how the choice of theoretical PMS evolutionary models affects disk dissipation timescales, the Age_{JX} method is applied to the MYStIX and SFiNCs YSOs using a number of different models.

We start with four different sets of stellar evolutionary models: Siess et al. (2000)[hereafter Siess00]; Baraffe et al. (2015)[hereafter Baraffe15]; Dotter (2016) and Choi et al. (2016)[hereafter MIST]; and Feiden et al. (2015) and Feiden (2016)[hereafter Feiden16]. A quick examination of

these models’ evolutionary isochrones placed on the $L_{bol} - T_{eff}$ diagram suggests that, within the locus of the MYStIX/SFiNCs YSOs, the predictions of the Baraffe15 and MIST models are in good agreement with each other (figure not shown). Due to a poorer-sampled published model grid, compared to MIST, the Baraffe15 model is omitted from further consideration. Compared to Siess00, newer generations of standard evolutionary models, such as Baraffe15 and MIST, with improved microphysics (including updated solar abundance scale, linelists, atmospheric convection parameters) predict systematically younger ages.

The Age_{JX} estimates for MYStIX and SFiNCs clusters based on the Siess00 model are already reported in Getman et al. (2014, 2018). Here we refer to these ages as Age_{JX} -Siess00. Next, we recalculate cluster ages using MIST as an underlying evolutionary model and following the same Age_{JX} procedure detailed in Getman et al. (2014). Here we refer to these ages as Age_{JX} -MIST. Briefly, the L_X -Mass relationship of Telleschi et al. (2007) is recalibrated by comparing the (T_{eff}, L_{bol}) measurements for Taurus X-ray emitting PMS stars (Güdel et al. 2007) to the MIST models. The X-ray luminosities of all Age_{JX} stars in MYStIX and SFiNCs are then converted to stellar masses. The differences between the resulting MIST and Siess00 based stellar masses are no more than 15%. Comparison of absolute J -band magnitudes and masses with the MIST evolutionary tracks yields ages for individual stars. Cluster ages are then calculated as median ages of all Age_{JX} stellar cluster members. Statistical errors on cluster ages are calculated as 68% confidence intervals using nonparametric bootstrap resampling. The bootstrap case resampling takes into account any forms of observed scatter; thus all sources of the scatter including the uncertainties on individual source extinctions, stellar masses, and local distances within the cluster (described in §§3.3 and 5 in Getman et al. 2014) are treated naturally. Bootstrap does not treat “systematic” uncertainties, such as the uncertainty in the knowledge of PMS evolutionary models or uncertainty on the distance from the Sun to the region (the latter is discussed in §5 in Getman et al. 2014); such effects globally shift age scales.

The Dartmouth stellar evolution model grid (Dotter et al. 2008) extended to the PMS phase is used as a basis for the Feiden16 models (Feiden et al. 2015). Two versions of the Feiden16 models are provided, “non-magnetic” and “magnetic” (Feiden 2016). The published model grid is rather poorly sampled ($\Delta t = 0.5$ Myr) with no predictions for photometric magnitudes. Thus, the usage of the Age_{JX} method is not feasible here; and instead we opt for a simple age rescaling technique. In this approach, 5,000 young stars within the parameter ranges of the MYStIX/SFiNCs- Age_{JX} stars are simulated on the L_{bol} versus T_{eff} diagram. Their ages are then derived using both the MIST and Feiden16 models. The resulting Feiden16 versus MIST age relationships are approximated by linear functions using standard major axis regression: $t_{F16, non-magnetic} = 0.35 + 0.94 \times t_{MIST}$ and $t_{F16, magnetic} = 0.59 + 2.00 \times t_{MIST}$.

Fig. 2 exemplifies comparison of the standard MIST and “magnetic” Feiden16 models. Compared to MIST, the Feiden16 “magnetic” models predict systematically higher (by a factor of 1.6) masses and older (by a factor of 2–3) ages. Following the above equations, the Age_{JX} -MIST ages for the MYStIX/SFiNCs clusters are then transformed to Age -

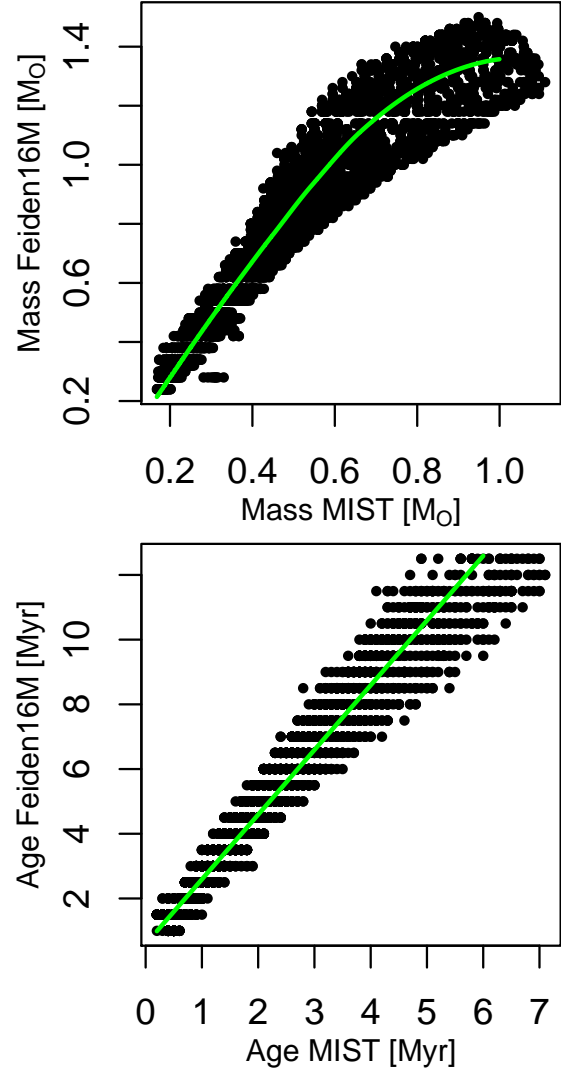


Figure 2. Comparison of the non-magnetic MIST (Dotter 2016; Choi et al. 2016) and magnetic Feiden16 (Feiden et al. 2015; Feiden 2016) PMS evolutionary models. Stellar masses (upper panel) and stellar ages (lower panel) resulted from the model fitting of simulated stars on the (L_{bol}, T_{eff}) diagram. The green curves are polynomial and linear (standard major axis) regression fits for the mass and age data, respectively. The polynomial and linear fits were obtained using the *R*(R Core Team 2014) functions *loess* and *lmodel2*, respectively.

Feiden16 cluster ages. The “non-magnetic” Feiden16 cluster ages are omitted from further consideration because they only slightly differ from the MIST ages ($< 30\%$ for 1 Myr and $< 10\%$ for > 2 Myr clusters) and are systematically lower than the Siess00 ages. In contrast, the “magnetic” Feiden16 cluster ages appear significantly higher than the MIST and Siess00 ages; we refer to these hereafter as Age -Feiden16M.

For all MYStIX/SFiNCs clusters, three types of cluster ages are reported in Table 1: old generation standard Siess00 (Age_{JX} -Siess00), new generation standard MIST (Age_{JX} -MIST), and new generation magnetic Feiden16 (Age -Feiden16M).

2.4 Stellar mass sensitivity

Given that disks around YSOs are detected using infrared excess, for a given infrared limiting magnitude, disk-bearing YSOs will be more readily detected than disk-free ones. Ignoring this sensitivity difference could lead to an erroneously high estimate of disk fraction—and therefore disk longevity—that reflects the underdetection of low-mass, disk-free YSOs. Note that this effect will manifest even if disk longevity does not vary with host star mass, and could wrongly lead to an *apparent* dependency of disk fraction on stellar mass.

In order to ensure that disk fractions are calculated within a similar range of stellar mass for each cluster, we choose a sensitivity limit for each cluster in the following way. Approximate stellar mass estimates are obtained based on star locations in the J versus $J - H$ color–magnitude diagram and theoretical stellar model tracks derived by [Siess et al. \(2000, for \$M_\star < 7 M_\odot\$ \)](#) and [Bressan et al. \(2012, for \$M_\star > 7 M_\odot\$ stars\)](#). The reddening law of [Rieke & Lebofsky \(1985\)](#) is used to deredden the star positions to the intrinsic pre-main sequence model colors, assuming a single age (Age_{JX} -Siess00) for all the stellar members of a cluster. These mass estimates are subject to significant uncertainties and may be incompatible with individual masses obtained by other methods such as optical spectroscopy ([Kuhn et al. 2010](#)). However, the analysis of disk longevity as a function of stellar mass presented in Section 3.3.2 makes use of large stellar mass bins, so precise estimates of mass for individual objects are not required.

Once stellar masses have been calculated, we compare the stellar mass distributions of disk-bearing and disk-free YSOs in each of our 69 clusters. For each cluster, we iteratively remove the lowest-mass YSO in the combined disk-bearing and disk-free sample until the Kolmogorov–Smirnov two-sample p -value exceeds 0.1. This yields a minimum mass cutoff M_{cut} for each cluster in order to ensure similar mass distributions and mass sensitivities for disk-bearing and disk-free YSOs. As mentioned in the next subsection, for many clusters, no YSOs are removed because they already show similar mass completeness for their disk-bearing and disk-free YSOs. Fig. 3 shows empirical cumulative distribution functions (ECDFs) of stellar mass for disk-bearing and disk-free objects in Rosette Nebula cluster E (NGC 2244; [Kuhn et al. 2014](#)), illustrating the derivation of M_{cut} and the effect of imposing it. For MYStIX clusters, typical values of M_{cut} typically range from 0.1 to 0.2 M_\odot , while for SFINC clusters, minimum stellar masses in the sample reach $\sim 0.1 M_\odot$, but no M_{cut} was applied due to the similar mass distributions of disk-bearing and disk-free stars.

Resulting subsamples of disk-bearing and disk-free stars, with similarly shaped mass ECDFs, are not affected by the choice of PMS evolutionary models insofar as both disk-bearing and disk-free samples are subject to the same mass transformation when transitioning among different PMS models. The mass scale itself changes; it is roughly similar between the Siess00 and MIST models, but shifts to higher values upon switching to the Feiden16M model (§2.3).

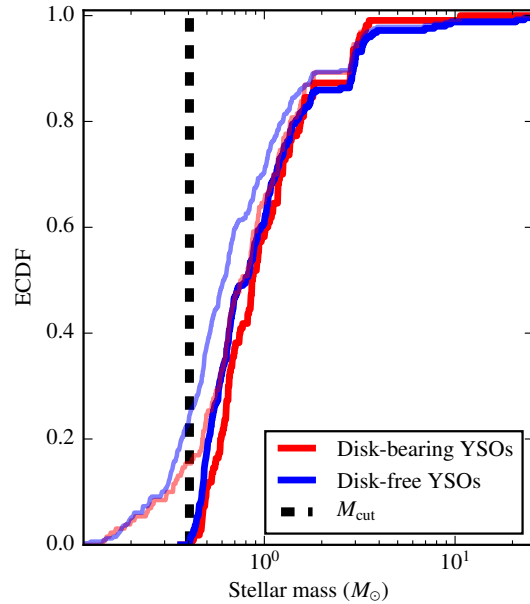


Figure 3. Comparison of stellar mass cumulative distributions for disk-bearing and disk-free YSOs in Rosette cluster E (NGC 2244), based on catalog YSO classifications. The thinner (translucent) and thicker (solid) lines indicate the mass distributions before and after the imposition of M_{cut} , respectively.

2.5 Summary of cluster data

Table 1 presents the cluster data.

Table 1. Properties of 69 MYStIX and SFiNCs clusters. This version of the table lists 69 entries (one per cluster) corresponding to the membership case with α_{IRAC} -based classification and probable protostars included. This table is available in its entirety (69×4 entries) in the Supplementary Materials. That is, the on-line table version gives four entries per cluster, one for each of the four membership permutations yielded by using two different YSO classification schemes (YSO Classes = Catalog and YSO Classes = α_{IRAC}) and including and excluding probable protostars. Here, Column 1: Cluster of interest. Column 2: Distances from the Sun, taken from Feigelson et al. (MYStIX; 2013) and Getman et al. (SFiNCs; 2017). Columns 3-5: Cluster ages using three different PMS evolutionary models. Columns 6-7: Minimum mass cut-off and median stellar mass in a cluster (based on the Siess00 age scale). Columns 8-9: Numbers of disk-bearing (N_{disk}) and disk-free (N_{nodisk}) YSOs after the imposition of M_{cut} . Column 10: Inferred disk fraction $f_{disk} = N_{disk}/(N_{disk} + N_{nodisk})$.

Region/Cluster	D	Age_{JX} Siess00	Age_{JX} MIST	Age Feiden16M	M_{cut} Siess00	Median mass Siess00	N_{disk}	N_{nodisk}	f_{disk}
(1)	(kpc) (2)	(Myr) (3)	(Myr) (4)	(Myr) (5)	(M_{\odot}) (6)	(M_{\odot}) (7)	(8)	(9)	(10)
MYStIX									
Eagle/A	1.75	2.4±1.0	2.0±0.8	4.5	0.95	1.24	3	13	0.19 ^{+0.12} _{-0.19}
Eagle/B	1.75	2.1±0.1	1.5±0.1	3.6	0.25	1.17	295	348	0.46 ^{+0.04} _{-0.04}
Eagle/D	1.75	2.5±0.2	1.6±0.2	3.8	0.16	1.47	151	153	0.50 ^{+0.06} _{-0.06}
Flame/A	0.414	0.8±0.2	0.4±0.1	1.5	0.10:	0.38	101	41	0.71 ^{+0.08} _{-0.07}
Lagoon/A	1.3	2.2±0.2	1.7±0.1	4.0	0.18:	0.69	16	11	0.59 ^{+0.19} _{-0.16}
Lagoon/C	1.3	1.6±0.2	1.0±0.3	2.7	0.11:	1.13	19	12	0.61 ^{+0.17} _{-0.15}
Lagoon/E	1.3	1.9±0.2	1.4±0.2	3.4	0.11:	1.06	34	44	0.44 ^{+0.10} _{-0.11}
Lagoon/F	1.3	2.3±0.1	1.8±0.2	4.2	0.12	0.96	108	153	0.41 ^{+0.06} _{-0.06}
Lagoon/H	1.3	2.1±0.4	1.3±0.3	3.2	0.10:	1.25	47	43	0.52 ^{+0.10} _{-0.10}
Lagoon/I	1.3	2.1±0.2	1.5±0.2	3.6	0.10:	0.97	79	85	0.48 ^{+0.08} _{-0.08}
Lagoon/J	1.3	2.7±0.2	1.9±0.3	4.4	0.11:	1.28	19	32	0.37 ^{+0.12} _{-0.14}
Lagoon/K	1.3	1.4±0.2	1.0±0.2	2.6	0.11:	1.19	60	28	0.68 ^{+0.10} _{-0.09}
M 17/D	2.0	1.1±0.2	0.7±0.1	2.0	0.12:	3.68	21	14	0.60 ^{+0.16} _{-0.14}
NGC 1893/A	3.6	3.5±1.0	2.7±0.9	5.9	0.19:	1.81	21	39	0.35 ^{+0.11} _{-0.13}
NGC 1893/B	3.6	2.6±0.3	2.0±0.3	4.7	0.09:	1.15	56	68	0.45 ^{+0.08} _{-0.09}
NGC 1893/I	3.6	2.8±0.6	1.9±0.3	4.3	0.12:	1.36	66	51	0.56 ^{+0.09} _{-0.09}
NGC 2264/E	0.913	3.2±0.5	2.4±0.7	5.4	0.10:	0.58	17	58	0.23 ^{+0.08} _{-0.11}
NGC 2264/J	0.913	1.6±0.7	1.2±0.6	3.0	0.10:	0.75	35	15	0.70 ^{+0.14} _{-0.11}
NGC 2264/K	0.913	2.2±0.3	1.5±0.2	3.6	0.09:	0.66	39	31	0.56 ^{+0.12} _{-0.11}
NGC 2362/B	1.48	2.9±0.2	2.1±0.2	4.8	0.09:	0.50	23	177	0.12 ^{+0.04} _{-0.05}
NGC 6334/B	1.7	2.3±0.4	1.8±0.5	4.1	0.17:	1.92	26	14	0.65 ^{+0.15} _{-0.13}
NGC 6334/J	1.7	1.5±0.4	0.9±0.4	2.3	0.11:	3.85	20	4	0.83 ^{+0.19} _{-0.10}
NGC 6334/L	1.7	0.7±0.3	0.4±0.2	1.4	0.39	1.60	20	1	0.95 ^{+0.18} _{-0.04}
NGC 6357/A	1.7	1.4±0.1	0.9±0.1	2.4	0.13:	1.58	60	64	0.48 ^{+0.09} _{-0.09}
NGC 6357/B	1.7	1.4±0.2	1.0±0.2	2.6	0.09:	1.46	94	62	0.60 ^{+0.08} _{-0.07}
NGC 6357/C	1.7	1.2±0.3	0.9±0.2	2.4	0.41	1.38	71	67	0.51 ^{+0.08} _{-0.08}
NGC 6357/E	1.7	1.4±0.4	0.9±0.3	2.3	0.14:	1.86	38	26	0.59 ^{+0.12} _{-0.11}
NGC 6357/F	1.7	1.5±0.2	1.0±0.2	2.6	0.11:	1.79	90	72	0.56 ^{+0.08} _{-0.07}
RCW 36/A	0.7	0.9±0.1	0.5±0.1	1.6	0.09:	0.35	105	24	0.81 ^{+0.08} _{-0.06}
Rosette/E	1.33	3.0±0.2	2.3±0.1	5.3	0.21	0.66	130	335	0.28 ^{+0.04} _{-0.04}
Rosette/L	1.33	2.7±0.7	1.9±1.0	4.3	0.10:	0.81	136	95	0.59 ^{+0.06} _{-0.06}
Rosette/M	1.33	1.9±0.4	1.4±0.3	3.3	0.11:	0.81	43	8	0.84 ^{+0.12} _{-0.08}
Rosette/N	1.33	1.3±1.4	0.7±1.0	2.0	0.12:	0.68	14	15	0.48 ^{+0.17} _{-0.17}
W 40/A	0.5	0.8±0.1	0.4±0.1	1.5	0.10:	0.53	123	33	0.79 ^{+0.07} _{-0.06}

Region/Cluster	D	Age_{JX} Siess00	Age_{JX} MIST	Age Feiden16M	M_{cut} Siess00	Median mass Siess00	N_{disk}	N_{nodisk}	f_{disk}
(1)	(kpc) (2)	(Myr) (3)	(Myr) (4)	(Myr) (5)	(M_{\odot}) (6)	(M_{\odot}) (7)	(8)	(9)	(10)
SFINCs									
Be 59/A	0.9	1.8±0.2	1.4±0.2	3.3	0.10:	0.78	149	152	0.50 ^{+0.06} _{-0.06}
Be 59/B	0.9	2.2±0.4	1.6±0.3	3.8	0.75	1.59	35	60	0.37 ^{+0.09} _{-0.10}
Cep A/A	0.7	1.4±0.3	1.0±0.2	2.6	0.10:	0.38	50	27	0.65 ^{+0.11} _{-0.10}
Cep A/U	0.7	2.0±0.3	1.4±0.3	3.3	0.10:	0.43	29	57	0.34 ^{+0.09} _{-0.10}
Cep C/U	0.7	2.2±0.9	2.0±0.6	4.6	0.10:	0.47	26	33	0.44 ^{+0.12} _{-0.13}
Cep OB3b/A	0.7	2.2±0.2	1.9±0.2	4.4	0.09:	0.36	201	195	0.51 ^{+0.03} _{-0.05}
Cep OB3b/C	0.7	2.4±0.1	2.0±0.1	4.6	0.09:	0.44	284	324	0.47 ^{+0.04} _{-0.04}
Cep OB3b/U	0.7	3.4±0.4	2.5±0.6	5.6	0.10:	0.42	33	48	0.41 ^{+0.10} _{-0.11}
GGD 12-15/A	0.83	0.6±0.6	0.4±0.6	1.4	0.10:	0.34	44	11	0.80 ^{+0.12} _{-0.08}
GGD 12-15/U	0.83	2.5±0.5	2.2±0.4	5.0	0.11:	0.43	31	57	0.35 ^{+0.09} _{-0.10}
IC 348/B	0.3	2.5±0.1	2.0±0.2	4.6	0.09:	0.36	91	129	0.41 ^{+0.06} _{-0.07}
IC 348/U	0.3	3.8±0.4	3.4±0.6	7.4	0.11:	0.35	11	27	0.29 ^{+0.12} _{-0.16}
IC 5146/B	0.8	1.5±0.2	1.2±0.2	3.1	0.10:	0.57	88	37	0.70 ^{+0.09} _{-0.07}
IC 5146/U	0.8	2.6±0.5	2.0±0.3	4.6	0.30	0.67	37	34	0.52 ^{+0.11} _{-0.11}
IRAS 00013+681/A	0.9	1.8±1.8	1.2±1.4	3.0	0.18	0.68	24	9	0.73 ^{+0.12} _{-0.13}
IRAS 20050+2720/U	0.7	3.3±0.4	2.6±0.4	5.8	0.57	0.99	8	20	0.29 ^{+0.13} _{-0.18}
LkH α 101/A	0.51	1.5±0.3	1.0±0.3	2.6	0.09:	0.37	78	62	0.56 ^{+0.08} _{-0.08}
LkH α 101/U	0.51	2.2±0.6	1.7±0.5	4.0	0.10:	0.34	23	22	0.51 ^{+0.14} _{-0.14}
Mon R2/A	0.83	1.2±0.1	0.9±0.1	2.4	0.09:	0.28	65	13	0.83 ^{+0.10} _{-0.07}
Mon R2/U	0.83	1.7±0.2	1.4±0.2	3.3	0.09	0.47	134	74	0.64 ^{+0.07} _{-0.06}
NGC 1333/A	0.235	2.5±1.2	1.2±1.5	3.0	0.09:	0.17	16	6	0.73 ^{+0.21} _{-0.14}
NGC 1333/B	0.235	1.7±0.3	1.3±0.3	3.2	0.09:	0.18	29	15	0.66 ^{+0.15} _{-0.12}
NGC 2068/B	0.414	1.2±0.2	0.7±0.1	2.0	0.10:	0.43	57	34	0.63 ^{+0.10} _{-0.09}
NGC 2068/D	0.414	1.0±0.3	0.6±0.2	1.8	0.11:	0.59	23	11	0.68 ^{+0.17} _{-0.13}
NGC 2068/U	0.414	2.3±0.4	1.4±0.5	3.4	0.09:	0.41	37	40	0.48 ^{+0.11} _{-0.11}
OMC 2-3/U	0.414	1.7±0.2	1.2±0.2	3.0	0.09:	0.32	81	100	0.45 ^{+0.07} _{-0.07}
ONC Flank N/A	0.414	1.7±0.2	1.2±0.2	3.0	0.13	0.52	80	104	0.43 ^{+0.07} _{-0.07}
ONC Flank S/A	0.414	1.6±0.2	1.1±0.1	2.8	0.09:	0.41	114	122	0.48 ^{+0.06} _{-0.06}
RCW 120/B	1.35	0.8±0.2	0.6±0.1	1.8	0.36:	1.41	41	32	0.56 ^{+0.11} _{-0.11}
RCW 120/C	1.35	0.7±0.4	0.5±0.3	1.6	0.19:	1.07	26	10	0.72 ^{+0.16} _{-0.12}
RCW 120/U	1.35	1.2±0.2	0.9±0.2	2.5	0.15:	0.91	22	40	0.35 ^{+0.11} _{-0.12}
Serpens Main/B	0.415	0.6±0.7	0.3±0.8	1.2	0.10:	0.64	14	10	0.58 ^{+0.19} _{-0.17}
Serpens Main/U	0.415	2.2±0.5	1.5±0.5	3.6	0.09:	0.19	17	19	0.47 ^{+0.15} _{-0.16}
Serpens South/U	0.415	1.8±0.8	1.7±0.6	4.0	0.11:	0.31	15	11	0.58 ^{+0.19} _{-0.17}
Sh 2-106/U	1.4	0.8±0.4	0.6±0.4	1.7	0.13:	0.60	49	43	0.53 ^{+0.10} _{-0.10}

Table 1 shows the following information for each of the 69 clusters studied in the current work: region name and cluster designation; three types of median ages (Age_{JX} -Siess00, Age_{JX} -MIST, and Age -Feiden16M); mass cut (M_{cut}) and median stellar mass based on the Siess00 model; the number of disk-bearing (N_{disk}) and disk-free (N_{nodisk}) YSOs after the imposition of M_{cut} ; and disk fraction ($N_{disk}/(N_{disk}+N_{nodisk})$). In the more complete, on-line version of Table 1, each cluster has four entries, one for each of the four permutations yielded by using two different YSO classification schemes (catalog classes versus α_{IRAC} -based) and including and excluding probable protostars.

A cluster designation of “U” for a SFiNCs cluster indicates the unclustered component of a region. An M_{cut} value suffixed by a “:” indicates that no YSOs were removed from the sample according to the process described in the previous subsection, in which case the given value of M_{cut} indicates the lowest stellar mass in the sample for that cluster. Disk fraction uncertainties are Wilson confidence intervals for confidence level 0.05 (Wilson 1927; Brown et al. 2001). Other properties of these SFiNCs and MYStIX clusters can be found in Getman et al. (2018), Kuhn et al. (2014), Kuhn et al. (2015a), and Kuhn et al. (2015b).

3 RESULTS

In most of this section, we explore the effects of initial disk fraction (§§3.1.1 and 3.1.2), star-forming environment (§3.1.3), and stellar mass (§§3.3.1 and 3.3.2) on disk longevity, employing age and mass results inferred from a single PMS evolutionary model, namely the Siess00 model. The effect of different PMS evolutionary models on disk longevity estimates is examined in §3.2 using the Siess00, MIST, and Feiden16M models.

3.1 Disk fraction versus age

3.1.1 With assumption of 100% initial disk fraction

Here we produce a disk evolution plot resembling that of Haisch et al. (2001b) and other researchers. Cluster disk fraction as a function of Age_{JX} -Siess00 for 69 MYStIX and SFiNCs clusters is shown in Fig. 4. The four figure versions (available in the Supplementary Materials) reflect the four permutations of our analysis methods: two YSO classification schemes and two rules regarding the inclusion of probable protostars (§ 2.2). We perform a Gauss–Newton least-squares fit of an exponential function $f_{disk} = f_0 \times e^{-t/\tau}$ (with the mean lifetime τ as a free parameter) to each of the 8 datasets (MYStIX and SFiNCs separately for each of the four membership permutations), assuming initial disk fraction $f_0 = 100\%$. The results are summarized in Table 2, along with the total number of disk-bearing and disk-free YSOs included in each analysis, as well as the sum of the squared residuals (SSR) for each exponential fit. The estimated disk half-life $t_{1/2} = \tau \times \ln(2)$ depends somewhat on the YSO classification scheme used, as well as on whether probable protostars are included in the sample, however the variation among these age estimates does not vary beyond their 95% confidence intervals (shown in Table 2). The goodness of fit is better for SFiNCs regions, and is typically

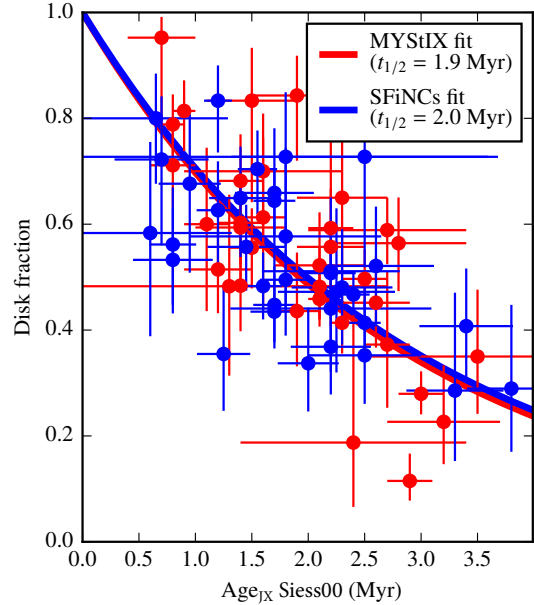


Figure 4. Disk fraction versus Age_{JX} -Siess00 for 69 MYStIX and SFiNCs clusters (red and blue points, respectively). The current figure exhibits results for one of the four membership permutations, that is, the α_{IRAC} -based YSO classification with probable protostars included. Figure panels showing disk fraction as a function of age for the other three permutations (based on catalog YSO classification with/without probable protostars included and based on the SED slope YSO classification when probable protostars are excluded) are provided in the Supplementary Materials. Vertical error bars show Wilson binomial confidence intervals for confidence level 0.05.

Table 2. Disk longevity estimates ($f_0 = 100\%$).

Project	YSO classes	Incl. possible protostars?	N_{disk}	N_{nodisk}	$t_{1/2}$ (Myr)	SSR
(1)	(2)	(3)	(4)	(5)	(6)	(7)
MYStIX	Catalog	N	1329	1606	$1.7^{+0.3}_{-0.2}$	0.90
MYStIX	Catalog	Y	1523	1675	$1.9^{+0.3}_{-0.3}$	0.95
MYStIX	α_{IRAC}	N	1924	2229	$1.8^{+0.2}_{-0.2}$	0.53
MYStIX	α_{IRAC}	Y	2180	2236	$1.9^{+0.3}_{-0.2}$	0.61
SFiNCs	Catalog	N	1971	1778	$2.1^{+0.3}_{-0.2}$	0.61
SFiNCs	Catalog	Y	2088	1761	$2.2^{+0.2}_{-0.2}$	0.55
SFiNCs	α_{IRAC}	N	1924	1971	$1.9^{+0.2}_{-0.2}$	0.59
SFiNCs	α_{IRAC}	Y	2062	1988	$2.0^{+0.2}_{-0.2}$	0.54

slightly better for the analyses using α_{IRAC} -based YSO classifications compared with those using catalog classifications.

3.1.2 Without assumption of 100% initial disk fraction

We explore the possibility that the zero-age disk fraction f_0 is less than 100%. That is, some stars would be born without dusty circumstellar disks, or lose these disks very rapidly (< 0.5 Myr). As in the previous subsection, we fit exponential functions, this time with f_0 as an additional parameter, using the adaptive nonlinear least-squares algorithm of Dennis et al. (1981). Results are shown in Table 3. For MYStIX

Table 3. Disk longevity and initial disk fraction estimates ($f_0 < 100\%$).

Project (1)	YSO classes (2)	Incl. possible protostars? (3)	$t_{1/2}$ (Myr) (4)	f_0 (5)	SSR (6)
MYStIX	Catalog	N	$2.2^{+2.0}_{-0.7}$	$0.84^{+0.16}_{-0.21}$	0.79
MYStIX	Catalog	Y	$2.3^{+2.2}_{-0.7}$	$0.87^{+0.13}_{-0.22}$	0.88
MYStIX	α IRAC	N	$1.8^{+0.6}_{-0.2}$	$1.00^{+0.00}_{-0.18}$	0.53
MYStIX	α IRAC	Y	$1.9^{+0.5}_{-0.2}$	$1.00^{+0.00}_{-0.13}$	0.61
SFiNCs	Catalog	N	$3.5^{+3.9}_{-1.2}$	$0.77^{+0.16}_{-0.14}$	0.43
SFiNCs	Catalog	Y	$3.2^{+2.7}_{-1.0}$	$0.83^{+0.16}_{-0.14}$	0.43
SFiNCs	α IRAC	N	$3.2^{+2.9}_{-1.0}$	$0.75^{+0.16}_{-0.14}$	0.43
SFiNCs	α IRAC	Y	$2.9^{+2.2}_{-0.9}$	$0.81^{+0.17}_{-0.15}$	0.44

clusters, the exponential half-lives do not differ significantly from those reported in Table 2, though the uncertainties become considerably larger; the initial disk fractions remain consistent with 100%. For SFiNCs clusters, the estimated half-lives are longer than those shown in Table 2, but no more than 2σ . In the two SFiNCs analyses where probable protostars are excluded, the upper 95% confidence intervals for f_0 only reach the low-90% range, which leaves room for the possibility that not all YSOs begin with a hot inner dust disk.

The large uncertainties on the disk half-life estimates shown in Table 3 stem from not having clusters in our sample that are both younger than 0.5 Myr and significantly older than the estimated e -folding times. Future works that examine disk longevity over a larger age range and have much richer homogeneous cluster samples should omit the assumption of 100% disk fraction at zero age, as well as explore other parametrizations of disk longevity, given that there is no physical basis for assuming an exponential decay.

3.1.3 Dependence on star-forming environment

Using the MYStIX and SFiNCs datasets, we attempt to test whether disks in the richer star-forming environments targeted by the MYStIX survey evolve differently from disks in the more sparse environments seen in SFiNCs fields. In particular, MYStIX clusters are often dominated by multiple O stars while SFiNCs clusters are generally dominated by a single massive star, typically a late-O or early-B.

Previous observations and theory suggest no strong effects by OB photoevaporation and/or dynamical interactions of cluster members on the inner parts of circumstellar disks. For instance, the results of Richert et al. (2015) suggest that external photoevaporation by OB stars does not affect the presence of infrared excess (nor is it likely to be based on theory, which does not predict significant truncation closer than ~ 100 AU to a disk’s host star; e.g., Anderson et al. 2013). Meanwhile, theory regarding disk truncation due to dynamical encounters among YSOs does not predict disk depletion much closer to the star than ~ 100 AU, and certainly not within the few-AU orbital radii associated with near-/mid-infrared excess (Portegies Zwart 2016; Vincke & Pfalzner 2016).

We find that the estimated values of $t_{1/2}$ and f_0 shown in Tables 2 and 3 do not differ beyond the expected statistical error between MYStIX and SFiNCs. Thus our data

Table 4. Disk longevity from the use of different PMS evolutionary models.

Project (1)	PMS evolutionary model (2)	YSO classes (3)	Incl. possible protostars? (4)	$t_{1/2}$ (Myr) (5)	SSR (6)
MYStIX+SFiNCs	Siess00	Catalog	N	1.9 ± 0.2	2.23
MYStIX+SFiNCs	Siess00	Catalog	Y	2.0 ± 0.2	1.52
MYStIX+SFiNCs	Siess00	α IRAC	N	1.8 ± 0.1	1.64
MYStIX+SFiNCs	Siess00	α IRAC	Y	1.9 ± 0.2	1.15
MYStIX+SFiNCs	MIST	Catalog	N	1.4 ± 0.1	2.44
MYStIX+SFiNCs	MIST	Catalog	Y	1.5 ± 0.2	1.66
MYStIX+SFiNCs	MIST	α IRAC	N	1.3 ± 0.1	1.67
MYStIX+SFiNCs	MIST	α IRAC	Y	1.4 ± 0.1	1.17
MYStIX+SFiNCs	Feiden16M	Catalog	N	3.4 ± 0.3	2.06
MYStIX+SFiNCs	Feiden16M	Catalog	Y	3.6 ± 0.4	1.43
MYStIX+SFiNCs	Feiden16M	α IRAC	N	3.2 ± 0.2	1.46
MYStIX+SFiNCs	Feiden16M	α IRAC	Y	3.5 ± 0.3	1.04

provide no evidence for distinctive dissipation timescales of disks in different star-forming environments.

3.2 Effect of PMS evolutionary models on disk longevity

Here we investigate the effect of uncertainty in our knowledge of PMS evolution on disk longevity. We study disk fraction as a function of age using three different sets of cluster ages: the traditional Age_{JX} -Siess00, the new Age_{JX} -MIST with improved microphysics, and the new Age -Feiden16M that include “radius inflation” due to magnetic fields (§2.3). This analysis is applied to the combined MYStIX+SFiNCs sample of 69 clusters using four different membership permutations (Table 4). Using the nonlinear weighted Gauss-Newton least-squares method, the datasets are fit with an exponential function $f_{disk} = f_0 \times e^{-t/\tau}$ with the mean lifetime τ as a free parameter and the initial disk fraction (f_0) fixed at 100%.

Fig. 5 and Table 4 show that even though the goodness of fit is better for the cases with “possible protostars included”, the variations in $t_{1/2}$ due to different membership permutations are small ($< 15\%$ of a value) and are comparable to the statistical errors.

In contrast, the choice of different PMS models has a much stronger effect (70%-170%) on estimated $t_{1/2}$. The magnetic PMS models of Feiden (2016) lead to significantly longer disk dissipation timescales ($t_{1/2, Feiden16M} \sim 3.5$ Myr) compared to those of the non-magnetic models ($t_{1/2, MIST, Siess00} \sim 1.3 - 2.0$ Myr). Clearly the choice of stellar evolutionary models, especially when magnetic fields are included, have a major effect on the inferred half-life of inner disks.

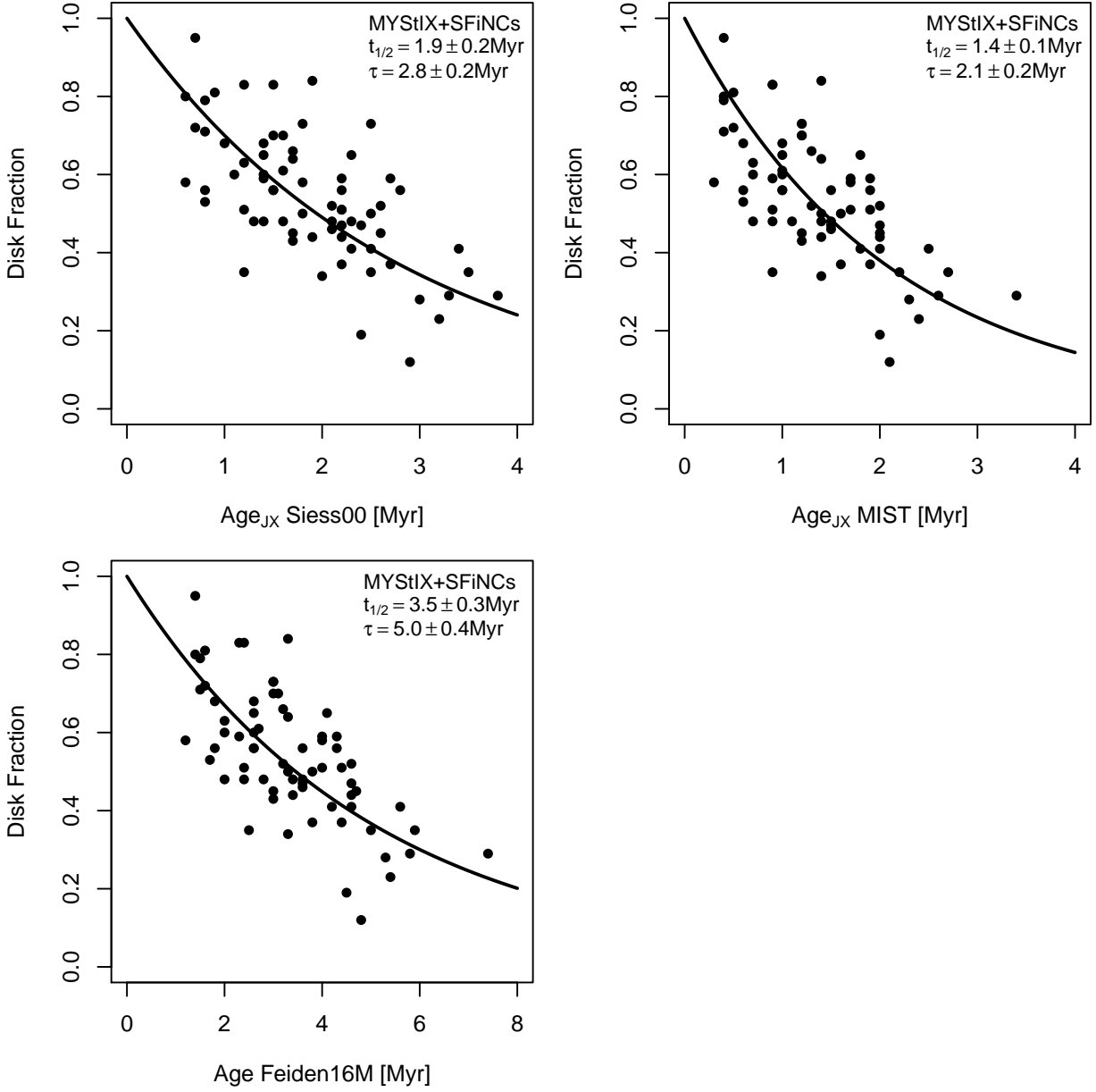


Figure 5. Disk fraction as a function of age using 3 types of cluster ages (Age_{JX} -Siess00, Age_{JX} -MIST, and Age -Feiden16M). The underlying dataset (black points) is the combined MYStIX+SFiNCs sample of 69 clusters. The current figure exhibits results for one of the four membership permutations, that is, the α_{IRAC} -based YSO classification with probable protostars included. Figure panels showing disk fraction as a function of age for the other three permutations are provided in the Supplementary Materials. The black lines represent the best model fits. The figure legends provide disk dissipation timescales resulting from the fits to an exponential model.

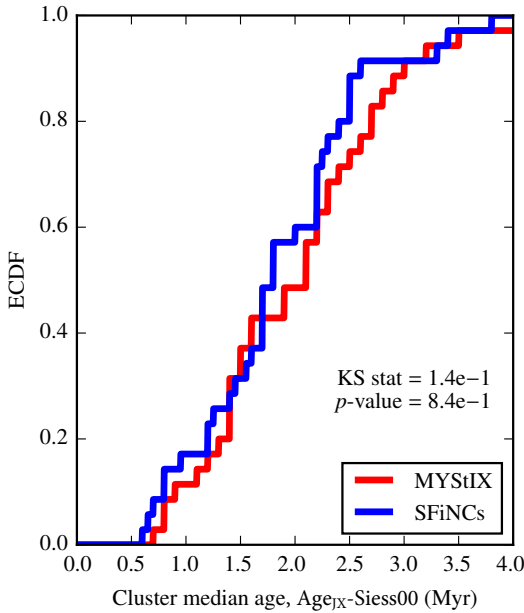


Figure 6. ECDF of median cluster ages ($Age_{JX-Siess00}$) for MYStIX (red) and SFiNCs (blue).

3.3 The role of stellar mass

Several previous works have indicated that disks survive longer around lower mass stars than around higher mass stars (Haisch et al. 2001a; Carpenter et al. 2006; Luhman & Mamajek 2012; Ribas et al. 2015).

In Section 3.3.1, we compare the properties of MYStIX and SFiNCs regions in order to determine differences in disk fraction due to the greater prevalence of higher mass stars in MYStIX than SFiNCs samples. In Section 3.3.2, we analyze the combined MYStIX and SFiNCs samples by binning YSOs according to age ($Age_{JX-Siess00}$) and stellar mass rather than by cluster.

3.3.1 Comparing MYStIX and SFiNCs clusters

We perform several comparisons of MYStIX and SFiNCs cluster properties. First, in Fig. 6, we compare ECDFs of median cluster ages (based on the Siess00 model) for MYStIX and SFiNCs. The ages of the MYStIX and SFiNCs cluster samples are similar.

Fig. 7 shows cluster disk fraction (across entire mass range and mass-stratified), median stellar mass (based on the Siess00 model), and median stellar mass by YSO type for the following analysis schemes, in order: catalog YSO classifications and excluding probable protostars; catalog YSO classifications and including probable protostars; α_{IRAC} -based YSO classifications and excluding probable protostars; and α_{IRAC} -based YSO classifications and including probable protostars.

The upper left panels of Fig. 7 show only modest differences in the distributions of disk fractions between MYStIX and SFiNCs clusters, which appear to stem largely from the presence of a handful of MYStIX clusters with low disk fractions. This is consistent with the similarity of the estimates of exponential disk half-life shown in Table 2, and does not

provide strong evidence for differential disk longevity between sparse (SFiNCs) and rich (MYStIX) star-forming regions.

The upper right panels of Fig. 7 show ECDFs of median cluster stellar mass for MYStIX and SFiNCs (YSO mass derivations are discussed in § 2.5). MYStIX clusters have higher median masses for two reasons. First, MYStIX clusters are more distant, therefore a given magnitude limit in a given near-infrared band will translate into a higher stellar mass. Second, MYStIX clusters are richer and therefore physically contain more of the rare high-mass stars.

The lower left panels of Fig. 7 show ECDFs of subcluster median stellar mass separately for disk-bearing and disk-free YSOs, and separately for MYStIX and SFiNCs (median masses are calculated after M_{cut} has been applied). The disk-bearing and disk-free distributions are quite close to each other within both MYStIX and SFiNCs while the distributions between the two projects are quite different.

The lower right panels of Fig. 7 show ECDFs of disk fraction stratified by mass, separately for SFiNCs and MYStIX clusters. To mitigate the small number statistics issue (some clusters have only a few stars with $M > 2 M_{\odot}$) the mass cutoff is chosen here as $1 M_{\odot}$. The figure shows no differences in the distributions of disk fractions between higher- and lower-mass stars when using the α_{IRAC} -based YSO classifications. Only modest differences in the distributions of disk fractions for SFiNCs stars are present when using the Catalog YSO classifications; with a hint of possible age dependence — the SFiNCs clusters with higher disk fractions for more massive stars are, on average, slightly younger than the SFiNCs clusters with lower disk fractions for more massive stars. But this age difference is not statistically significant.

To summarize, for the same age range, MYStIX clusters have higher median masses (upper right and lower left panels of Fig. 7) than SFiNCs clusters. Any mass dependence of disk longevity thus should be apparent in the upper left and lower right panels of Fig. 7. The similarities of disk fractions between SFiNCs and MYStIX clusters when using the α_{IRAC} -based YSO classifications and only modest differences for some cluster sub-samples when using the Catalog YSO classifications show that disk fraction is not strongly dependent on stellar mass. We explore this result in more detail in the following subsection.

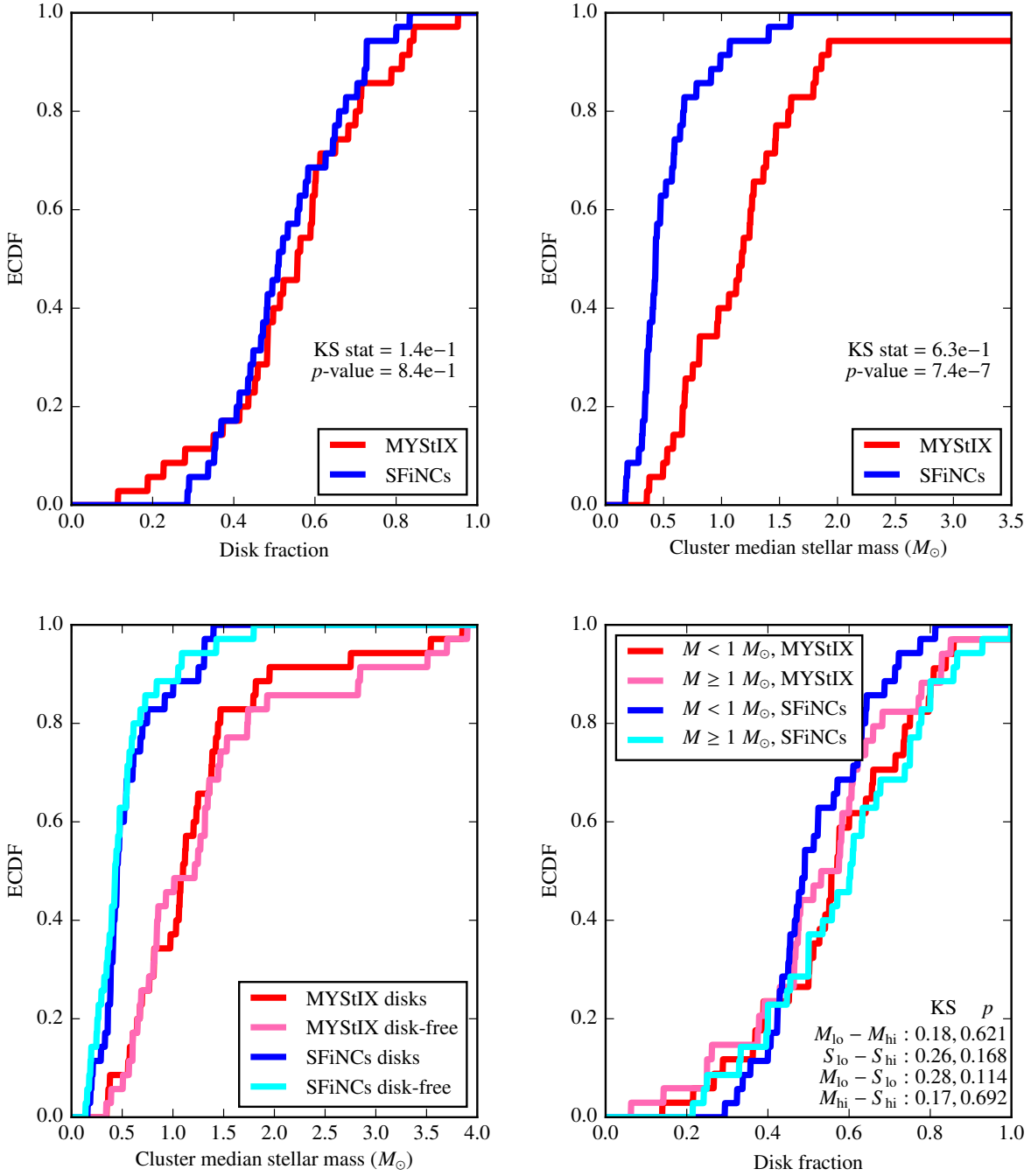


Figure 7. Cumulative distributions of cluster disk fraction (upper left panel), cluster median stellar mass (based on the Siess00 model; upper right panel), cluster median stellar mass separately for disk-bearing and disk-free YSOs (lower left panel), and disk fraction separately for low-mass ($M < 1 M_{\odot}$) and high-mass ($M \geq 1 M_{\odot}$) YSOs (lower right panel), separately for MYStIX and SFiNCs. The current figure shows a membership case based on α_{IRAC} value and probable protostars included ($\alpha_{IRAC} > 0$). Figure panels showing cumulative distributions of disk fraction and median mass for the other three membership permutations are provided in the Supplementary Materials.

3.3.2 Disk longevity as a function of host star mass

For the stellar population in the relatively old Upper Sco association ($t \sim 11$ Myr; Pecaut et al. 2012), Carpenter et al. (2006); Luhman & Mamajek (2012) find that the more massive stars ($M > 1.2 M_{\odot}$) have a lower fraction of inner primordial disks. For the younger star-forming regions, NGC 1333 and IC 348 ($t \lesssim 3$ Myr), Luhman et al. (2016) find no signs of disk fraction variations within the spectral type range from L-type to B-type. Similarly, Kennedy & Kenyon (2009) find no significant differences in disk fraction between the $M < 1.5 M_{\odot}$ and $M > 1.5 M_{\odot}$ members of the younger, $t \lesssim 3$ Myr, stellar populations in Taurus, Cha I, and IC 348, but they provide observational evidence of stellar mass-dependent disk dispersal for older ($t > 3$ Myr) populations. In contrast, Ribas et al. (2015) suggest that the differences in the primordial disk fraction between the higher-mass ($> 2 M_{\odot}$) and lower-mass ($< 2 M_{\odot}$) stars are present even in younger ($t \lesssim 3$ Myr) regions, such as in the combined sample of Cha I, Cha II, CrA, Lupus, NGC 1333, σ Ori, Serpens, and Taurus.

Physically, this implies either an increased disk depletion rate due to accretion, photoevaporation, and planet(esimal) formation for higher-mass host stars, or that initial disk fraction decreases with increasing stellar mass. In order to explore this question using the MYStIX and SFiNCs datasets, we place the YSOs that informed Fig. 4 into four stellar mass bins and four age bins; in other words, YSOs are now associated by age and mass, not by cluster. In this analysis, cluster ages and masses are derived based on the Siess00 model.

Disk fraction versus age for each of the four mass bins is shown in Fig. 8; the sample size within each mass bin is shown in the legend for each panel; with star numbers varying within the 1,300–2,800 range. The figure shows no statistically significant trends in disk fraction with stellar mass for young (< 4 Myr; assuming the Siess00 age scale) clusters.

Surveys exclusively using infrared data to detect and classify YSOs may be at risk of underestimating the number of disk-free YSOs and thereby overestimating disk fraction (and subsequently disk longevity) among low-mass stars. By applying M_{cut} (§ 2.4), we ensure similar sensitivity to disk-bearing and disk-free YSOs.

However, our survey may have a bias against disk-free intermediate-mass stars because it relies on X-ray selection. It is well known that the X-ray sensitivity diminishes towards mid-B and mid-A type stars (e.g., Stelzer et al. 2009; Güdel & Nazé 2009; Drake et al. 2014). Such an X-ray sensitivity bias towards A- and B-type stars might lead to overestimation of disk fractions for our $> 2 M_{\odot}$ stellar sample in Fig. 8, and thus prevent us from detecting the effect of lower disk fractions in higher mass stars reported in a number of previous disk fraction studies.

On the other hand, we consider our non-detection of such a trend to be consistent with the recent findings of Luhman et al. (2016) for the young ($t \lesssim 3$ Myr on the Siess00 age scale) IC 348 and NGC 1333 star-forming regions, which show no statistically significant variations in disk fraction for objects with spectral types between L0 and late B, although their sample of stellar members with spectral types earlier than K6 ($M \gtrsim 1 M_{\odot}$) is relatively small. Meanwhile, for the

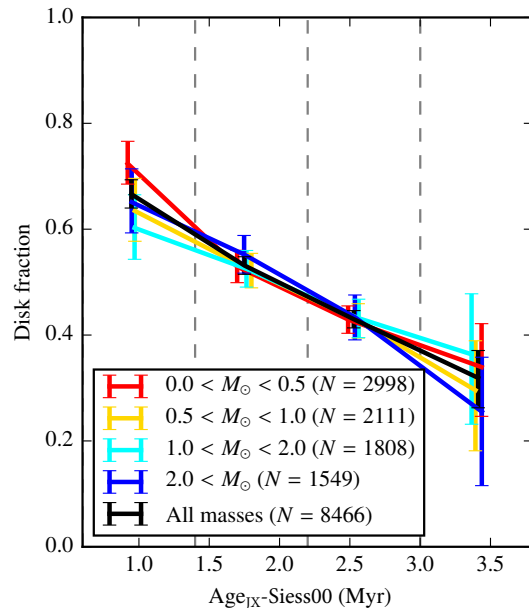


Figure 8. Disk fraction as a function of age ($Age_{JX-Siess00}$) for four bins of stellar mass, combining data across all 69 MYStIX and SFiNCs clusters. The current figure exhibits results for one of the four membership permutations, that is, the α_{IRAC} -based YSO classification with probable protostars included. Figure panels showing disk fraction as a function of age for the other three permutations (based on catalog YSO classification with/without probable protostars included and based on the SED slope YSO classification when probable protostars are excluded) are provided in the Supplementary Materials. Vertical error bars are Wilson binomial confidence intervals for significance level 0.05. Dashed lines indicate age bin boundaries.

much older population in the Upper Sco association ($t \sim 11$ Myr; Pecaut et al. 2012), Luhman & Mamajek (2012) report a trend of a decreasing disk fraction from M-type to B–G type stars. These results may point to an increased disk depletion rate in higher-mass stars throughout their disk evolution.

In Fig. 8, for the cases of catalog-based YSO classification with and without probable protostars, we see diminished disk fractions for young (youngest two age bins), intermediate-mass ($1\text{--}2 M_{\odot}$) stars. To explore this, we first redo the analysis shown in Fig. 8 separately for MYStIX and SFiNCs (results not shown); the effect seems to emerge from the MYStIX sample alone. We also find that the increase in disk fraction going from the catalog-based to the SED-based classifications comes from a gain in disk-bearing YSOs, not a loss of disk-free ones. Given the high nebulosity in many MYStIX regions, it is reasonable to suspect that contamination due to emission from polycyclic aromatic hydrocarbons (PAHs) reduces the sensitivity of YSO classification based on SED models toward disk-bearing YSOs. Indeed, we find that if we reproduce the analysis shown in Fig. 8 while excluding the three most heavily contaminated MYStIX clusters identified by Richert et al. (2015) based on $8 \mu\text{m}$ background levels, the effect in question disappears. This would seem to explain the large differences in M_{cut} between the catalog YSO classifications and SED slope-based YSO clas-

sifications seen in Table 1, such as for NGC 6357 B, where the SED slope-based classifications achieve stellar mass completeness down to $\sim 0.1 M_{\odot}$, as opposed to $\sim 0.6 M_{\odot}$ for the catalog classifications. X-ray measurements do not suffer from this problem, therefore the number of disk-free YSOs in the young-age, intermediate-mass regime in question does not change significantly between the catalog-based to SED-based classifications (Fig. 8).

Richert et al. (2015) find that in several distant, rich, OB-dominated MYStIX regions, the large point spread functions of early O stars in *Spitzer*/IRAC bands diminish sensitivity toward infrared excess from disk-bearing YSOs (whereas disk-free objects are still detected by X-rays). To ensure that the lower disk fraction for high-mass YSOs seen in Fig. 8 is not due to this effect, we perform the same analysis again, but now excluding OB-dominated regions identified as problematic by Richert et al. (2015), namely M 17 and NGC 6357. The results are not affected, apart from the effect discussed in the previous paragraph.

4 CONCLUSIONS

4.1 Summary of results

In this work, we have studied circumstellar disk longevity in 69 young stellar clusters by combining X-ray and infrared data and studying cluster disk fraction as a function of age. We have applied homogeneously-derived cluster ages (based on the Age_{JX} method) and carefully accounted for the relative sensitivity to different clusters in the infrared and X-ray bands. The SFiNCs and MYStIX samples collectively exceed previous cluster samples by more than a factor of three.

Our data show that disk longevity estimates are strongly sensitive to the choice of PMS evolutionary model, but are not so sensitive to YSO classification scheme, initial disk fraction, stellar mass, and star-forming environment.

Our analysis has yielded IRAC half-lives of $t_{1/2} \sim 1.3 - 2$ Myr based on the non-magnetic Siess00 and MIST models, but much longer half-lives of $t_{1/2} \sim 3.5$ Myr based on the magnetic Feiden16M model. According to the relationship $\tau = t_{1/2}/\ln(2)$, these half-lives $t_{1/2}$ translate into mean lifetimes of $\tau \sim 1.9 - 2.9$ Myr based on the non-magnetic Siess00 and MIST models, and $\tau \sim 5.0$ Myr based on the magnetic Feiden16M model.

Half-life estimates change only somewhat when the initial disk fraction is allowed to vary below 100%, however the constraints on initial disk fraction and especially half-life are weak due to the limited age range of our sample.

We find no statistically significant evidence that disk fraction varies with stellar mass within the first few Myr of life. However, this result may be inaccurate for MYStIX and SFiNCs stars more massive than $2 M_{\odot}$ due to reduced X-ray sensitivity towards mid-B and mid-A type stars.

Our data do not provide clear evidence that disk longevity depends on the surrounding star-forming environment.

4.2 Comparison with previous works

Our finding of a $t_{1/2} \sim 2$ Myr half-life (mean lifetime $\tau \sim 2.9$ Myr) for disks based on the Siess00 age scale agrees

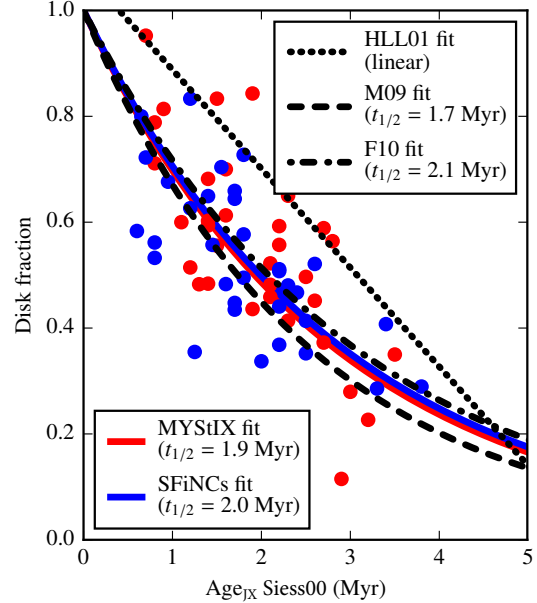


Figure 9. Disk fraction versus age (based on the Siess00 models) for 69 MYStIX and SFiNCs clusters, along with results of Haisch et al. (2001b, HLL01), Mamajek (2009, M09), and Fedele et al. (2010, F10). The MYStIX and SFiNCs fits are shown for the case of an SED slope-based YSO classification with probable protostars ($\alpha_{IRAC} > 0.0$) included.

closely with those of several previous works (Mamajek 2009; Fedele et al. 2010; Ribas et al. 2014), which generally included heterogeneous compilations of cluster ages based on old-generation PMS evolutionary models. Fig. 9 shows a comparison of our results with those of Haisch et al. (2001b), Mamajek (2009), and Fedele et al. (2010). Our finding of a $t_{1/2} \sim 3.5$ Myr half-life (mean lifetime $\tau \sim 5.0$ Myr) based on the Feiden16M age scale is consistent with that of the recent work of Pecaute & Mamajek (2016). Detailed comparison with these studies follows.

(i) **Haisch et al. (2001b).** Fig. 9 shows that our disk fractions (based on the Siess00 model) are systematically lower than those of Haisch et al. (2001b, HLL01). One reason is differing disk classifications. The cluster IC 348 is found in both the SFiNCs and HLL01 samples, making it a useful example for exploring this possibility. In IC 348, $\sim 40\%$ of objects classified as disk-bearing by HLL01 are classified as disk-free in the SFiNCs catalog. This indicates that the *JHKL*-based color-color diagram approach to identifying disk-bearing YSOs yields different results from those provided by longer-wavelength ($3-8 \mu\text{m}$) data. A similar disparity in the disk classifications is provided by HLL01 and Lada et al. (2006), the latter of which makes use of *Spitzer* photometry; approximately a third of the YSOs shared between the HLL01 and Lada et al. (2006) catalogs have disparate classifications. Lada et al. (2006) notice that the $K-[3.6]$ colors of the stars in their work “appear to be bluer than the $K-L$ colors of Haisch et al.,” for unclear reasons. The SFiNCs *Spitzer*-IRAC photometric measurements are consistent with those of Lada et al. (see Figure A3 in Getman et al. 2017). It is worth noting that our estimated disk frac-

tion for IC 348 agrees closely with the estimate of [Luhman et al. \(2016\)](#). The level of $3.6 \mu\text{m}$ variability estimated by [Flaherty et al. \(2013\)](#) is small (standard deviations of order hundredths of a magnitude), and is therefore unlikely to lead to significant misclassification of YSOs.

A second possible explanation for the systematically higher disk fractions reported by HLL01 is related to their imposition of different mass limits for disk-bearing and disk-free objects as we discuss in §2.4. HLL01 use the analysis of [Haisch et al. \(2001a\)](#) to derive the disk fraction of IC 348. [Haisch et al. \(2001a\)](#) claim to be complete down to $L \sim 12$ for disk-bearing and disk-free objects. However, in J and H bands, which trace the stellar photosphere and therefore serve as proxies for stellar mass, the sample of [Haisch et al. \(2001a\)](#) is substantially deeper for disk-bearing objects. L -band measurements are sensitive to the presence of a disk, therefore the imposition of a similar limit for disk-bearing and disk-free objects in the L band will be biased toward finding disks, leading to a significant overestimation of disk fraction. Excluding sources with $H > 12$ for the [Haisch et al. \(2001a\)](#) catalog in IC 348 lowers the disk fraction by a factor of $\sim 11\%$. Correction for both effects (discrepancy in the $K - L$ color and imposition of the L -band cuts) is needed to bring the HLL01 disk fraction in agreement with ours.

(ii) [Mamajek \(2009\)](#). He performs a literature compilation of heterogeneous sets of ages and disk fractions for 22 nearby young stellar clusters. His disk indicator is based on the combination of spectroscopic accretion and photometric IR excess signatures. Mamajek introduces the exponential decay formalism. For the compiled dataset he obtains a mean-lifetime of $\tau = 2.5$ Myr ($t_{1/2} = 1.7$ Myr). MYStIX/SFiNCs Siess00-based disk dissipation timescale of $t_{1/2} \sim 2$ Myr is consistent with that of Mamajek despite the heterogeneity of Mamajek's dataset.

(iii) [Fedele et al. \(2010\)](#). They find that disk half-lives estimated based on spectroscopic indicators of accretion ($\tau = 2.3$ Myr; $t_{1/2} = 1.6$ Myr) are shorter than those based on infrared excess ($\tau = 3.0$ Myr; $t_{1/2} = 2.1$ Myr) to identify disks. The MYStIX/SFiNCs Siess00 result of $t_{1/2} \sim 2$ Myr agrees with their estimate of disk lifetime based on infrared excess.

(iv) [Pecaut et al. \(2012\)](#); [Pecaut & Mamajek \(2016\)](#). They find that for the Scorpius–Centaurus OB association, the age estimates of low-mass (K- and M-type) PMS stars are systematically lower (by a factor of two) compared to those of higher-mass (G- and F-type) PMS and massive B-type main-sequence stars. This age discrepancy is likely related to the problem of “radius inflation” in low-mass PMS stars (§1) and can be mitigated by introducing magnetic effects in PMS models ([Somers & Pinsonneault 2015](#); [Feiden 2016](#)). For the Upper Sco (US), Upper Centaurus-Lupus (UCL), and Lower Centaurus-Crux (LCC) sub-regions of the OB association, [Pecaut & Mamajek \(2016\)](#) adopt HRD-based ages inferred for intermediate-mass G- and F-type PMS stars using the median age values among the output of four different, relatively modern PMS evolutionary models, including [Dotter et al. \(2008\)](#) and Baraffe15. Using these three clusters (US, UCL, and LCC), [Pecaut & Mamajek \(2016\)](#) estimate disk dispersal half-life of $t_{1/2} = 3.3$ Myr ($\tau = 4.7$ Myr).

The agreement with the MYStIX/SFiNCs half-life of $t_{1/2} \sim 3.5$ Myr (based on the Feiden16M time scale) is some-

what remarkable, considering the paucity of the Pecaut et al. cluster sample (only three clusters), as well as the following difference in disk indicators. As a disk indicator [Pecaut & Mamajek \(2016\)](#) use *WISE* photometry, which goes significantly farther into the infrared ($3.4\text{--}22 \mu\text{m}$), compared to *Spitzer*-IRAC employed by MYStIX/SFiNCs ($3.6\text{--}8 \mu\text{m}$). By probing cooler, farther-out regions of disks, we would expect the Pecaut et al. study to arrive at longer disk dispersal timescales, but this has not occurred.

(v) [Ribas et al. \(2014\)](#). The last possibility discussed above is supported by disparate estimates of disk lifetimes for shorter wavelength ($3.4\text{--}12 \mu\text{m}$; $\tau \lesssim 3$ Myr) and longer wavelength ($22\text{--}24 \mu\text{m}$; $\tau \gtrsim 4$ Myr) observations ([Ribas et al. 2014](#)), reflecting differential evolution for different grain sizes and different regions of disks. [Lada et al. \(2006\)](#) classify several objects in IC 348 as disk-bearing that are designated as disk-free in the SFiNCs catalog. [Lada et al. \(2006\)](#) use $24 \mu\text{m}$ *Spitzer* data to help identify disks, suggesting that the use of ($<8 \mu\text{m}$) infrared data as in the current work will fail to identify transition disks due to their lack of a hot inner component.

(vi) [Bell et al. \(2013\)](#). They introduce new semi-empirical model isochrones to correct the aforementioned problem of radius inflation and systematically lower ages for low-mass stars derived using standard PMS models ([Pecaut et al. 2012](#); [Pecaut & Mamajek 2016](#)). Since a treatment of low-mass stellar ages is applied in Bell et al., we would expect to have our MYStIX/SFiNCs disk half-life of $t_{1/2} \sim 3.5$ Myr (based on the Feiden16M timescale), as well as that of [Pecaut & Mamajek \(2016\)](#), to be comparable with that of Bell et al. However, some complications arise.

For 13 clusters, Bell et al. combine their new age estimates with *Spitzer*-based disk fractions compiled from the literature to obtain a disk dissipation timescale. Judging from their Figure 18, Bell et al. report a disk half-life of $\sim 5 - 6$ Myr. Two issues arise here. First, Bell et al. do not provide any formal exponential fits to the data. By applying the non-linear Gauss–Newton least-squares method to fit an exponential function $f_{disk} = f_0 \times e^{t/\tau}$ (with $f_0 = 100\%$) to the data given in their Figure 18, we derive a disk half-life of $t_{1/2} \sim 3$ Myr ($\tau \sim 4.3$ Myr). This is rather inconsistent with their own reported value of $\sim 5 - 6$ Myr.

Second, several regions are found in both the [Bell et al. \(2013\)](#) dataset and the combined MYStIX and SFiNCs dataset. These regions are Eagle Nebula, Lagoon Nebula, NGC 2264 (part of Rosette Nebula), IC 5146, Cep OB3b, and IC 348. Surprisingly, for the first four regions, these are *Age_{JX}*-Siess00 estimates and not *Age*-Feiden16M that appear to agree fairly well with those reported by [Bell et al. \(2013\)](#). MYStIX/SFiNCs *Age*-Feiden16M estimates are systematically higher than those of Bell et al.

For Cep OB3b and IC 348, our *Age_{JX}*-Siess00 and *Age*-Feiden16M ages are in the 2.5–4.5 Myr range, as opposed to the Bell et al. estimates of 6 Myr. While any number of factors affect age estimates, one partial explanation may be the disparate distance estimates between [Bell et al. \(2013\)](#) and the current work for Cep OB3b and IC 348, while the distance estimates agree more closely for the other four regions. The $\sim 20\%$ disagreement in distances for these two clusters is likely a major factor in explaining the age disparity. Tycho-*Gaia* parallax distances for several objects in IC 348 confirm the SFiNCs adopted distance of 300 pc, as

opposed to the distance of 250 pc adopted by Bell et al. (2013). As for Cep OB3b, Very Long Baseline Array parallax distances for two objects in Cep A—HW 2 and HW 9—are ~ 700 pc (Moscadelli et al. 2009; Dzib et al. 2011). Given the small (~ 10 pc) projected distance between Cep A and Cep OB3b (Sargent 1977), we conclude that the Bell et al. (2013) distance of 570 pc based on color–magnitude diagrams is likely to be a substantial underestimation of the true distance. If the ages of Bell et al. (2013) for these two clusters are replaced with their Age_{JX} -Siess00 values from SFiNCs, the exponential half-life for the data shown in Bell et al. (2013) Figure 18 further decreases from $t_{1/2} \sim 3$ Myr to $t_{1/2} \sim 2$ Myr (assuming 100% initial disk fraction). *Gaia* DR2 data will help to clarify these distance issues.

4.3 Suggestions for future work

To conclude, we distill the discussions of Sections 3 and 4 into suggestions for future studies of disk longevity.

(i) Large datasets using homogeneously-derived cluster ages, based on PMS evolutionary models whose predictions are consistent with observations, are imperative for deriving reliable estimates of disk lifetimes and initial disk fraction. Our current work employing the largest cluster dataset used in a study of this kind to date with homogeneous sets of cluster ages based on the old (Siess00) and modern (MIST, Feiden16M) sets of evolutionary models shows a strong effect of the choice of PMS models on the disk longevity estimates.

As discussed in Section 3.1.2, stronger constraints on disk lifetimes and initial disk fractions will require a sample that spans a range of stellar age longer than the characteristic timescale of disk evolution. A larger age range will also allow for non-exponential parametrizations of the data to be explored. A significant sample of stars across all masses will be needed in order to resolve the question raised by our results in Section 3.3 of whether disks around high-mass stars evolve similarly to those orbiting lower-mass stars.

(ii) Ensuring similar mass sensitivities for disk-bearing and disk-free sources is important for deriving reliable estimates of disk longevity and initial disk fraction, especially at older ages where disk fractions are low and subsequently sensitive to small differences in numbers of sources. Although we are concerned about this issue, it did not prove to be so important in other studies such as Mamajek (2009); Fedele et al. (2010); Ribas et al. (2014); Pecaut & Mamajek (2016) except for HLL01. Since these previous studies focus mainly on nearby star-forming regions, it is possible that within the datasets employed, the disk-free and disk-bearing stellar samples have similar mass distributions.

The detection of disk-free YSOs will be greatly facilitated by the use of X-ray data, as well as the use of higher-sensitivity infrared instruments such as those offered by the James Webb Space Telescope, especially for older objects with diminished X-ray luminosities. The imposition of consistent stellar mass sensitivity limits for disk-bearing and disk-free YSOs will be important for deriving strong constraints on disk lifetimes and initial disk frequencies, and also for exploring the role of stellar mass, cluster environment, and so on. Emission from polycyclic aromatic hydrocarbons in rich star-forming regions may pose a problem for ensuring consistent sensitivity toward disk-bearing and

disk-free stars even for high-mass stars. Ensuring consistent sensitivity at higher masses may be important for calculating disk fractions among older systems ($> 3 - 5$ Myr), where mass-dependent effects may emerge (based on the results of the current work, they do not seem to emerge for systems younger than a few Myr; however, our disk fractions inferred for $\gtrsim 2 M_{\odot}$ stars may be overestimated due to the diminished X-ray sensitivity in mid-B and mid-A type stars).

(iii) Future studies of disk fraction versus age should separately explore multiple indicators of disks (while using otherwise homogeneous methods). In particular, using a large range of infrared through sub-mm wavelengths, as well as spectroscopic indicators, will help to determine how different regions of disks evolve. Near-/mid-infrared ($1 - 8 \mu\text{m}$) data is important for probing the inner several AU of disks, providing constraints on the time available for the in situ formation of Earth analogs (though the presence of near-/mid-infrared excess does not necessarily indicate that a sufficient amount of dust for building a planet is available). Longer wavelength data, on the other hand, can provide insight into the evolution of the outer, cooler regions of disks, which appear to evolve more slowly (Ribas et al. 2014).

ACKNOWLEDGEMENTS

We thank the referee for his/her very helpful comments. We thank K. Luhman, E. Mamajek, M. Pecaut, G. Somers, and R. Jeffries for stimulating discussions. The MYStIX project is now supported by the *Chandra* archive grant AR7-18002X. The SFiNCs project is supported at Penn State by NASA grant NNX15AF42G, *Chandra* GO grant SAO AR5-16001X, *Chandra* GO grant GO2-13012X, *Chandra* GO grant GO3-14004X, *Chandra* GO grant GO4-15013X, and the *Chandra* ACIS Team contract SV474018 (G. Garmire & L. Townsley, Principal Investigators), issued by the *Chandra* X-ray Center, which is operated by the Smithsonian Astrophysical Observatory for and on behalf of NASA under contract NAS8-03060. The Guaranteed Time Observations (GTO) data used here were selected by the ACIS Instrument Principal Investigator, Gordon P. Garmire, of the Huntingdon Institute for X-ray Astronomy, LLC, which is under contract to the Smithsonian Astrophysical Observatory; Contract SV2-82024. This research has made use of NASA's Astrophysics Data System Bibliographic Services and SAOImage DS9 software developed by Smithsonian Astrophysical Observatory.

REFERENCES

- Alencar S. H. P., et al., 2010, *A&A*, **519**, A88
- Anderson K. R., Adams F. C., Calvet N., 2013, *ApJ*, **774**, 9
- Armitage P. J., 2011, *ARA&A*, **49**, 195
- Audard M., et al., 2014, *Protostars and Planets VI*, pp 387–410
- Bai X.-N., 2011, *ApJ*, **739**, 50
- Baraffe I., Chabrier G., Allard F., Hauschildt P. H., 1998, *A&A*, **337**, 403
- Baraffe I., Homeier D., Allard F., Chabrier G., 2015, *A&A*, **577**, A42
- Bell K. R., Cassen P. M., Klahr H. H., Henning T., 1997, *ApJ*, **486**, 372
- Bell C. P. M., Naylor T., Mayne N. J., Jeffries R. D., Littlefair S. P., 2013, *MNRAS*, **434**, 806

- Boss A. P., 2010, in AAS/Division for Planetary Sciences Meeting Abstracts #42. p. 1070
- Bouvier J., Cabrit S., Fernandez M., Martin E. L., Matthews J. M., 1993, *A&A*, **272**, 176
- Bressan A., Marigo P., Girardi L., Salasnich B., Dal Cero C., Rubele S., Nanni A., 2012, *MNRAS*, **427**, 127
- Broos P. S., et al., 2013, *ApJS*, **209**, 32
- Brown L. D., Cai T. T., DasGupta A., 2001, *Statist. Sci.*, **16**, 101
- Carpenter J. M., Mamajek E. E., Hillenbrand L. A., Meyer M. R., 2006, *ApJ*, **651**, L49
- Castelli F., Kurucz R. L., 2004, ArXiv Astrophysics e-prints,
- Choi J., Dotter A., Conroy C., Cantiello M., Paxton B., Johnson B. D., 2016, *ApJ*, **823**, 102
- Cody A. M., et al., 2014, *AJ*, **147**, 82
- Dennis Jr. J. E., Gay D. M., Walsh R. E., 1981, *ACM Trans. Math. Softw.*, **7**, 348
- Dotter A., 2016, *ApJS*, **222**, 8
- Dotter A., Chaboyer B., Jevremović D., Kostov V., Baron E., Ferguson J. W., 2008, *ApJS*, **178**, 89
- Drake J. J., Braithwaite J., Kashyap V., Günther H. M., Wright N. J., 2014, *ApJ*, **786**, 136
- Dzib S., Loinard L., Rodríguez L. F., Mioduszewski A. J., Torres R. M., 2011, *ApJ*, **733**, 71
- Fang Q., Herczeg G. J., Rizzuto A., 2017, *ApJ*, **842**, 123
- Fedele D., van den Ancker M. E., Henning T., Jayawardhana R., Oliveira J. M., 2010, *A&A*, **510**, A72
- Feiden G. A., 2016, *A&A*, **593**, A99
- Feiden G. A., Jones J., Chaboyer B., 2015, in van Belle G. T., Harris H. C., eds, Cambridge Workshop on Cool Stars, Stellar Systems, and the Sun Vol. 18, 18th Cambridge Workshop on Cool Stars, Stellar Systems, and the Sun. pp 171–176 ([arXiv:1408.1791](https://arxiv.org/abs/1408.1791))
- Feigelson E. D., et al., 2013, *ApJS*, **209**, 26
- Flaherty K. M., Muzerolle J., Rieke G., Gutermuth R., Balog Z., Herbst W., Megeath S. T., 2013, *AJ*, **145**, 66
- Getman K. V., Feigelson E. D., Sicilia-Aguilar A., Broos P. S., Kuhn M. A., Garmire G. P., 2012, *MNRAS*, **426**, 2917
- Getman K. V., et al., 2014, *ApJ*, **787**, 108
- Getman K. V., Broos P. S., Kuhn M. A., Feigelson E. D., Richert A. J. W., Ota Y., Bate M. R., Garmire G. P., 2017, *ApJS*, **229**, 28
- Getman K. V., Kuhn M. A., Feigelson E. D., Broos P. S., Bate M. R., Garmire G. P., 2018, "Young Star Clusters In Nearby Molecular Clouds", *MNRAS*, in press
- Güdel M., Nazé Y., 2009, *A&ARv*, **17**, 309
- Güdel M., et al., 2007, *A&A*, **468**, 353
- Gutermuth R. A., Megeath S. T., Myers P. C., Allen L. E., Pipher J. L., Fazio G. G., 2009, *ApJS*, **184**, 18
- Haisch Jr. K. E., Lada E. A., Lada C. J., 2001a, *AJ*, **121**, 2065
- Haisch Jr. K. E., Lada E. A., Lada C. J., 2001b, *ApJ*, **553**, L153
- Hernández J., Calvet N., Hartmann L., Briceño C., Sicilia-Aguilar A., Berlind P., 2005, *AJ*, **129**, 856
- Hernández J., Hartmann L., Calvet N., Jeffries R. D., Gutermuth R., Muzerolle J., Stauffer J., 2008, *ApJ*, **686**, 1195
- Hernández J., Morales-Calderon M., Calvet N., Hartmann L., Muzerolle J., Gutermuth R., Luhman K. L., Stauffer J., 2010, *ApJ*, **722**, 1226
- Jeffries R. D., 2017, preprint, ([arXiv:1709.01736](https://arxiv.org/abs/1709.01736))
- Jeffries R. D., et al., 2017, *MNRAS*, **464**, 1456
- Kennedy G. M., Kenyon S. J., 2009, *ApJ*, **695**, 1210
- Königl A., Salmeron R., 2011, The Effects of Large-Scale Magnetic Fields on Disk Formation and Evolution. pp 283–352
- Kraus A. L., Cody A. M., Covey K. R., Rizzuto A. C., Mann A. W., Ireland M. J., 2015, *ApJ*, **807**, 3
- Kuhn M. A., Getman K. V., Feigelson E. D., Reipurth B., Rodney S. A., Garmire G. P., 2010, *ApJ*, **725**, 2485
- Kuhn M. A., Getman K. V., Broos P. S., Townsley L. K., Feigelson E. D., 2013a, *ApJS*, **209**, 27
- Kuhn M. A., Povich M. S., Luhman K. L., Getman K. V., Busk H. A., Feigelson E. D., 2013b, *ApJS*, **209**, 29
- Kuhn M. A., et al., 2014, *ApJ*, **787**, 107
- Kuhn M. A., Getman K. V., Feigelson E. D., 2015a, *ApJ*, **802**, 60
- Kuhn M. A., Feigelson E. D., Getman K. V., Sills A., Bate M. R., Borissova J., 2015b, *ApJ*, **812**, 131
- Lada C. J., et al., 2006, *AJ*, **131**, 1574
- Luhman K. L., Mamajek E. E., 2012, *ApJ*, **758**, 31
- Luhman K. L., Esplin T. L., Loutrel N. P., 2016, *ApJ*, **827**, 52
- Lynden-Bell D., Pringle J. E., 1974, *MNRAS*, **168**, 603
- Lyra W., Johansen A., Klahr H., Piskunov N., 2008, *A&A*, **491**, L41
- Mamajek E. E., 2009, in Usuda T., Tamura M., Ishii M., eds, American Institute of Physics Conference Series Vol. 1158, American Institute of Physics Conference Series. pp 3–10 ([arXiv:0906.5011](https://arxiv.org/abs/0906.5011)), doi:10.1063/1.3215910
- Moscadelli L., Reid M. J., Menten K. M., Brunthaler A., Zheng X. W., Xu Y., 2009, *ApJ*, **693**, 406
- Naylor T., Broos P. S., Feigelson E. D., 2013, *ApJS*, **209**, 30
- Pecaut M. J., Mamajek E. E., 2016, *MNRAS*, **461**, 794
- Pecaut M. J., Mamajek E. E., Bubar E. J., 2012, *ApJ*, **746**, 154
- Portegies Zwart S. F., 2016, *MNRAS*, **457**, 313
- Povich M. S., et al., 2013, *ApJS*, **209**, 31
- Preibisch T., 2012, *Research in Astronomy and Astrophysics*, **12**, 1
- Pringle J. E., 1981, *ARA&A*, **19**, 137
- R Core Team 2014, R: A Language and Environment for Statistical Computing. R Foundation for Statistical Computing, Vienna, Austria, <http://www.R-project.org/>
- Ribas Á., Merín B., Bouy H., Maud L. T., 2014, *A&A*, **561**, A54
- Ribas Á., Bouy H., Merín B., 2015, *A&A*, **576**, A52
- Richert A. J. W., Feigelson E. D., Getman K. V., Kuhn M. A., 2015, *ApJ*, **811**, 10
- Rieke G. H., Lebofsky M. J., 1985, *ApJ*, **288**, 618
- Robitaille T. P., Whitney B. A., Indebetouw R., Wood K., Denzmore P., 2006, *ApJS*, **167**, 256
- Sargent A. I., 1977, *ApJ*, **218**, 736
- Shakura N. I., Sunyaev R. A., 1973, *A&A*, **24**, 337
- Siess L., Dufour E., Forestini M., 2000, *A&A*, **358**, 593
- Soderblom D. R., Hillenbrand L. A., Jeffries R. D., Mamajek E. E., Naylor T., 2014, *Protostars and Planets VI*, pp 219–241
- Somers G., Pinsonneault M. H., 2015, *ApJ*, **807**, 174
- Somers G., Stassun K. G., 2017, *AJ*, **153**, 101
- Stelzer B., Robrade J., Schmitt J. H. M. M., Bouvier J., 2009, *A&A*, **493**, 1109
- Strom K. M., Strom S. E., Edwards S., Cabrit S., Skrutskie M. F., 1989, *AJ*, **97**, 1451
- Telleschi A., Güdel M., Briggs K. R., Audard M., Palla F., 2007, *A&A*, **468**, 425
- Townsley L. K., Broos P. S., Garmire G. P., Bouwman J., Povich M. S., Feigelson E. D., Getman K. V., Kuhn M. A., 2014, *ApJS*, **213**, 1
- Vincke K., Pfalzner S., 2016, *ApJ*, **828**, 48
- Wilson E. B., 1927, Journal of the American Statistical Association, **22**, 209
- Youdin A. N., Goodman J., 2005, *ApJ*, **620**, 459

This paper has been typeset from a $\text{\TeX}/\text{\LaTeX}$ file prepared by the author.